4-2010

Synoptic Typing of Extreme Cool-Season Precipitation Events at St. John's, Newfoundland, 1979-2005

Shawn M. Milrad
McGill University, milrads@erau.edu

Eyad H. Atallah
McGill University

John R. Gyakum
McGill University

Scholarly Commons Citation

Milrad, S. M., Atallah, E. H., & Gyakum, J. R. (2010). Synoptic Typing of Extreme Cool-Season Precipitation Events at St. John's, Newfoundland, 1979-2005. *Weather and Forecasting, 25*(2). https://doi.org/10.1175/2009WAF2222301.1

Synoptic Typing of Extreme Cool-Season Precipitation Events at St. John's, Newfoundland, 1979–2005

SHAWN M. MILRAD, EYAD H. ATALLAH, AND JOHN R. GYAKUM

Department of Atmospheric and Oceanic Sciences, McGill University, Montreal, Quebec, Canada

(Manuscript received 13 May 2009, in final form 1 October 2009)

ABSTRACT

Quantitative precipitation forecasting (QPF) continues to be a significant challenge in operational forecasting, particularly in regions susceptible to extreme precipitation events. St. John's, Newfoundland, Canada (CYYT), is affected frequently by such events, particularly in the cool season (October–April).

The 50 median events in the extreme (>33.78 mm during a 48-h period) precipitation event category are selected for further analysis. A manual synoptic typing is performed on these 50 events, using two separate methodologies to partition events. The first method utilizes a Lagrangian backward air parcel trajectory analysis and the second method utilizes the evolution of dynamically relevant variables, including 1000–700-hPa horizontal temperature advection, 1000–700-hPa (vector) geostrophic frontogenesis, and 700–400-hPa absolute vorticity advection.

Utilizing the first partitioning method, it is found that south cases are characterized by a strong anticyclone downstream of St. John's, southwest events are synoptically similar to the overall extreme composite and are marked by a strong cyclone that develops in the Gulf of Mexico, while west events are characterized by a weak Alberta clipper system that intensifies rapidly upon reaching the Atlantic Ocean. The second partitioning method suggests that while cyclone events are dominated by the presence of a rapidly developing cyclone moving northeastward toward St. John's, frontal events are characterized by the presence of a strong downstream anticyclone and deformation zone at St. John's.

It is the hope of the authors that the unique methodology and results of the synoptic typing in this paper will aid forecasters in identifying certain characteristics of future precipitation events at St. John's and similar stations.

1. Introduction

Milrad et al. (2009) discuss the perils of quantitative precipitation forecasting (QPF) in regions susceptible to extreme precipitation events, even when the mass field forecasts are essentially correct, as was also discussed by Roebber and Bosart (1998) and Sisson and Gyakum (2004). Located at the confluence of several North American storm tracks (Milrad et al. 2009), Atlantic Canada (Fig. 1), and specifically, St. John's, Newfoundland, is a place that is particularly susceptible to extreme events during the cool season (Stewart et al. 1987), defined in this study as October–April, which can often produce flooding rains, paralyzing snow, and damaging winds. By selecting a station that has a very small seasonal window for convection, and limiting the events in this study to those that occur from October to April, the role of convection is mitigated, although the small possibility of convection playing a role in an October or April event exists.

In Milrad et al. (2009), three classes of precipitation events (extreme, moderate, and light) were identified at St. John's (CYYT) over a 27-yr (1979–2005) period. Here, an effort is made to further analyze the 50 extreme events used in the composite detailed in Milrad et al. (2009). These 50 events are distributed as follows: 6 events in January, 11 in February, 2 in March, 6 in April, 9 in October, 8 in November, and 8 in December.

The main objective of this paper is to identify important synoptic structures and precursors associated with various synoptic types and subcomposites of the 50 median extreme events defined in Milrad et al. (2009). This is achieved by performing a manual synoptic typing, utilizing two separate methodologies.

Corresponding author address: Shawn M. Milrad, Dept. of Atmospheric and Oceanic Sciences, McGill University, 805 Sherbrooke St. W, Montreal, QC H3A 2K6, Canada.
E-mail: shawn.milrad@gmail.com

DOI: 10.1175/2009WAF2222301.1

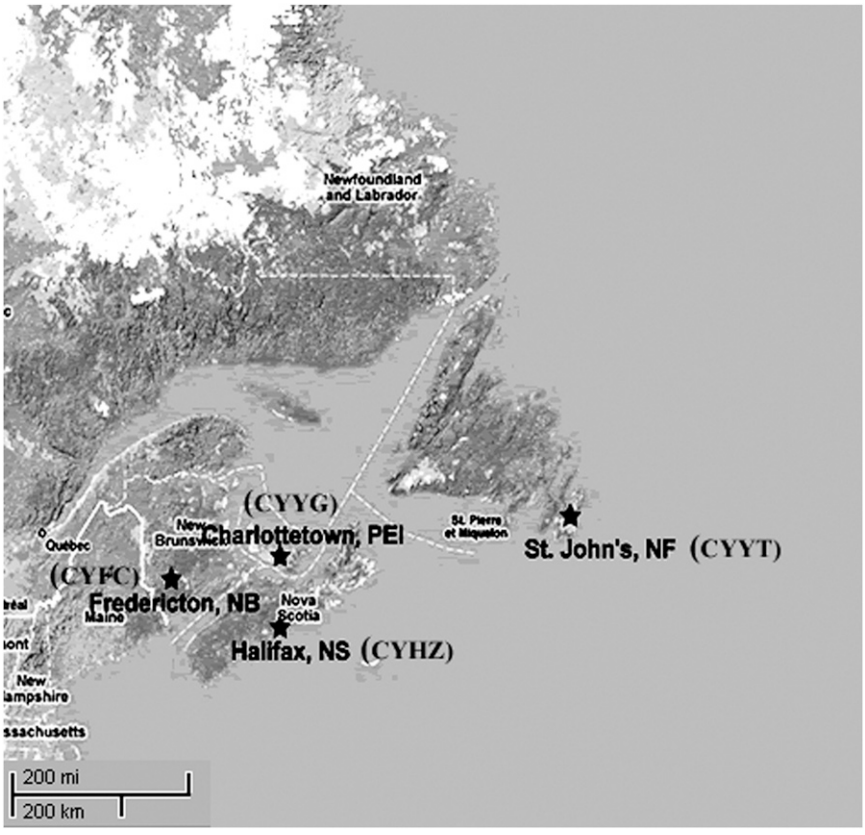

FIG. 1. The geography of Atlantic Canada, with the capital city of each province identified, and scale as shown.

Manual synoptic typing is not new in atmospheric science, and has been performed for surface and upper-air analyses of weather events in west Texas (Ladd and Driscoll 1980), an environmental baseline and air quality analysis in Louisiana (Muller 1977; Muller and Jackson 1985), and a synoptic climatology for the northeast Gulf of Alaska (Overland and Hiester 1980). Alternatively, automated synoptic typing, typically involving principal component analysis, has been used in countless studies, including Jones et al. (1993), Frakes and Yarnal (1997), and Sheridan (2002). Both Frakes and Yarnal (1997) and Sheridan (2002) argue that both manual and automated means of synoptic typing can sometimes be used in the same study and are useful for synoptic climatology studies.

2. Methodology and data

a. Methodology

The methodology used in this paper revolves around two means of manual typing: first, a 3D Lagrangian backward-trajectory analysis parses out events by air parcel source region, and, second, time series of three quasigeostrophic (QG) ascent-forcing parameters.

1) BACKWARD-TRAJECTORY ANALYSIS

Reap (1972) uses a primitive numerical model to compute 3D air parcel trajectories from wind forecasts to provide more guidance for severe storm prediction. Uccellini et al. (1985) used trajectories on an isentropic surface in an analysis of the Presidents' Day storm of 1979. In the late 1990s both Wernli and Davies (1997) and Wernli (1997) used a Lagrangian-based method to research the structure and dynamics of extratropical cyclogenesis. Wernli and Davies (1997) stated that 3D trajectories are useful in attaining ''i) the identification of the spatial coordinates and physical properties of the air parcels at the reference time (and) ii) the time-trace of the location and physical properties of the same air parcels for prior and/or subsequent time periods.''

Bao et al. (2006), Knippertz and Martin (2007), and Roberge et al. (2009) use a backward-trajectory analysis in studies of tropical moisture transport. Roberge et al. (2009) use trajectories as a partitioning tool for cases of tropical moisture transport into northwestern Canada.

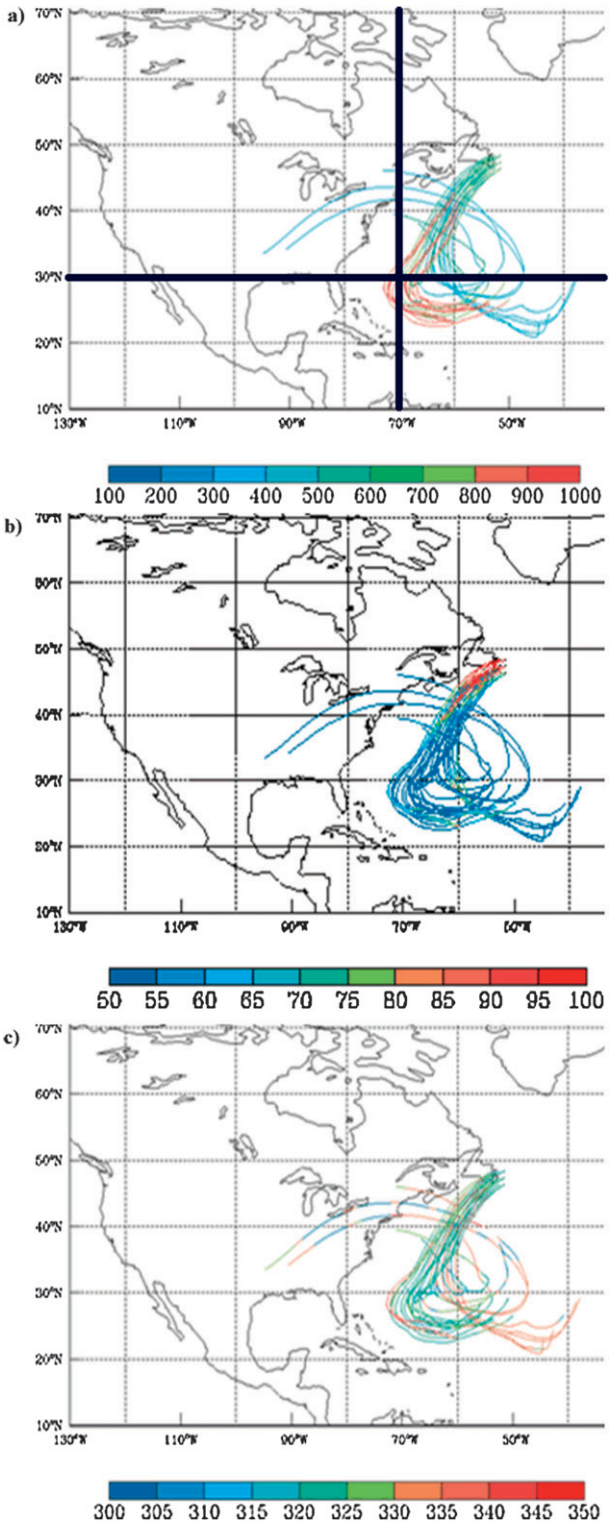

To partition the 50 extreme events by air parcel source region, 5-day (120 h) three-dimensional backward trajectories are analyzed using the National Centers for Environmental Prediction–National Center for Atmospheric Research (NCEP–NCAR) global reanalysis (Kalnay et al. 1996), starting at the beginning of the 6-h period of maximum recorded precipitation at St. John's ($t = 0$ h). Twenty-seven backward air parcel trajectories are initiated from a 3° × 3° box centered at 47°40′N, 52°50′W, roughly the location of St. John's International Airport (CYYT). The trajectories are computed simultaneously and end at 300, 500, or 700 hPa. These levels are chosen based on the fact that these air parcels generally have a history of ascent. As such, these trajectories often originate in the boundary layer in the time frame of the analyses. Three ending levels are displayed to show that trajectories that end at different levels often originate from the same source region up to 5 days prior to the precipitation event.

All 50 cases and the associated backward trajectories are also evaluated using higher-resolution North American Regional Reanalysis (NARR) data (Mesinger et al. 2006). Results indicate that the datasets produce backward trajectories that are very similar, and that the classifications established by the partitioning methodology in this paper are valid irrespective of which dataset is used.

2) QUASIGEOSTROPHIC FORCING

The second method of manual partitioning is based on time tendencies of three QG ascent forcing parameters at the station during the time of precipitation (midlevel vorticity advection, low-level horizontal temperature advection, and low-level geostrophic frontogenesis). The first two parameters are the first two forcing terms on the right-hand side of the quasigeostrophic omega equation [Eq. (1)]. The form of the QG omega equation used in this paper [Eq. (1)] is Eq. (5.6.11) in Bluestein (1992a), where (a) is the three-dimensional Laplacian of vertical motion (omega), (b) represents differential vorticity advection, and (c) is the horizontal Laplacian of

←

FIG. 2. Twenty-seven backward trajectories with the origin being 5 days earlier and the ending points at 300, 500, and 700 hPa at 0600 UTC 18 Oct 986. Ending points are distributed within a box whose corners are 48.4°N, 53.5°W and 46.4°N, 51.5°W. This is an example of a south event. Latitude 30°N and longitude 70°W are critical to the partitioning [set in boldface in (a)]. (a) The tracer used is pressure (hPa) where warm colors indicate closer to the surface. (b) Tracer used is relative humidity (%) where warm colors indicate values closer to 100%. (c) Tracer used is θ_e (K) where warm colors indicate greater values of θ_e.

temperature advection. In Eq. (1), f_0 is the Coriolis parameter, σ is the static stability parameter, ω is the vertical velocity in pressure coordinates, $\mathbf{v}_g$ is the geostrophic wind vector, $\nabla_p(\zeta_g + f)$ is the gradient of geostrophic absolute vorticity on a constant pressure surface, and R is the gas constant for dry air:

$$\underbrace{\left[\nabla_p^2 + \frac{f_0^2}{\sigma}\frac{\partial^2}{\partial p^2}\right]\omega}_{\text{(a)}} = \underbrace{-\frac{f_0}{\sigma}\frac{\partial}{\partial p}[-\mathbf{v}_g \cdot \nabla_p(\zeta_g + f)]}_{\text{(b)}} + \underbrace{\frac{R}{\sigma p}[-\nabla_p^2(-\mathbf{v}_g \cdot \nabla_p T)]}_{\text{(c)}}. \quad (1)$$

The third parameter is based on a diagnosis of the frontogenesis, which is defined by the expression found in Eq. (2). Equation (2), the vector frontogenesis is function, is Eq. (2.5.19) in Bluestein (1992b), where $\mathbf{F}_p$ is the vector frontogenesis function (defined by the time tendency of the potential temperature gradient, $\nabla_p\theta$). The frontogenesis is related to QG forcing for ascent via Eqs. (3) and (4), where Eq. (3) is Eq. (2.5.36) in Bluestein (1992b) and Eq. (4) is Eq. (5.7.58) in Bluestein (1992a). Equation (3) relates the geostrophic frontogenesis to **Q** vectors, where **Q** is the **Q** vector, p is the pressure, p_0 is some reference pressure, σ is the static stability parameter, and κ is R divided by C_p, the specific heat at constant pressure. Equation (4) states the **Q**-vector form of the inviscid adiabatic QG omega equation in which the sense of vertical motion is related to the divergence of the **Q** vector, which is supported by the assertion of Hoskins et al. (1978), which states that "in quasi-geostrophic theory … vertical velocity is forced solely by the divergence of **Q**":

$$\mathbf{F}_p = \frac{D_p}{Dt}\nabla_p\theta, \quad (2)$$

$$\mathbf{Q} = \frac{R}{\sigma p}\left(\frac{p}{p_o}\right)^{\kappa}\mathbf{F}_p, \quad (3)$$

$$\left(\nabla_p^2 + \frac{f_0^2}{\sigma}\frac{\partial^2}{\partial p^2}\right)\omega = -2\nabla_p \cdot \mathbf{Q}, \quad (4)$$

$$\mathbf{Q}_s = \left[\frac{\mathbf{Q} \cdot (k \times \nabla\theta)}{|\nabla\theta|}\right]\frac{k \times \nabla\theta}{|\nabla\theta|}, \quad \text{and} \quad (5)$$

$$\mathbf{Q}_n = \left(\frac{\mathbf{Q} \cdot \nabla\theta}{|\nabla\theta|}\right)\frac{\nabla\theta}{|\nabla\theta|}. \quad (6)$$

Finally, Keyser et al. (1988) suggest that the use of geostrophic frontogenesis as a diagnostic tool for quasigeostrophic forcing is incomplete without assessing the along-front and normal-to-front components of the frontogenesis. To this end, these components have been evaluated using Eqs. 6.50 and 6.49 from Martin (2006), which are Eqs. (5) and (6), respectively. These equations allow for the diagnosis of the along-front ($\mathbf{Q}_s$) and normal-to-front ($\mathbf{Q}_n$) components of the **Q** vector, which are proportional to the corresponding components of frontogenesis (Keyser et al. 1988). Keyser et al. (1988) also point out that the parallel component of frontogenesis is related to forcing associated with temperature advections in association with a synoptic-scale wave and the normal component of frontogenesis relates to mesoscale forcing. Results of these diagnostics are detailed in section 4a.

b. Data

This study utilizes 6-hourly precipitation data for St. John's, obtained from the Environment Canada 6-h corrected precipitation database. The corrected precipitation data are based on work done by Mekis and Hogg (1999), whereby the data have been adjusted to accurately reflect precipitation gauge changes, wind conditions, and changes in station location. In addition, all precipitation data in this study are observed in liquid equivalent form (i.e., no data were acquired using ruler methods), limiting errors associated with frozen precipitation. The NCEP–NCAR reanalysis is used as the dataset for all synoptic-scale composite and anomaly plots. The backward-trajectory analysis is based on a FORTRAN program originally developed at the State University of New York at Albany (A. Aiyyer 2008, personal communication). Most calculations and analyses in this study are performed and displayed using the General Meteorological Package, version 5.7.4 [updated from the original package devised by Koch et al. (1983)], a data manipulation and visualization software package.

3. Synoptic typing I: Backward-trajectory analysis

a. Partitioning methodology

The area of trajectory origin is used to partition the 50 events into three categories: south, southwest, and west. Of the 50 extreme events, 11 are classified as south cases, 31 as southwest cases, and 8 as west cases.

Figure 2 depicts 1 of 11 south trajectory cases from an event in October 1986, with the onset of heaviest precipitation ($t = 0$ h) being 0600 UTC 18 October 1986 and

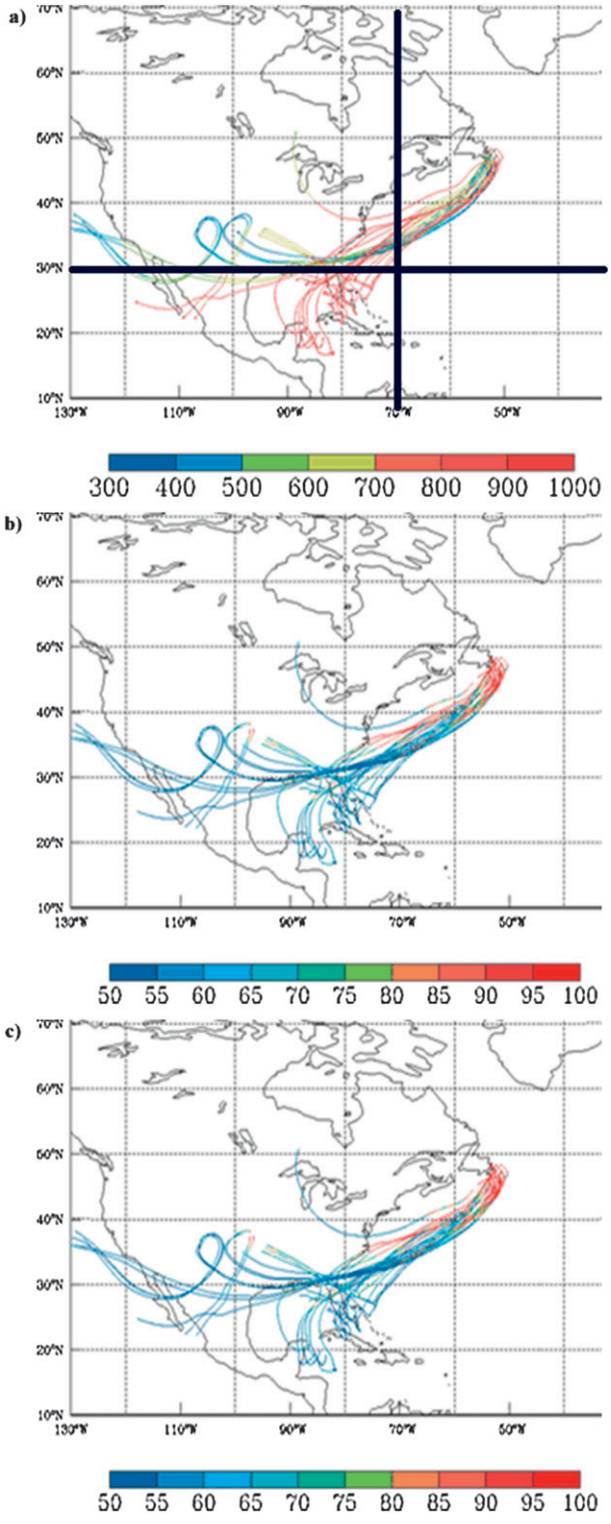

FIG. 3. As in Fig. 2, but for 0000 UTC 21 Apr 1988.

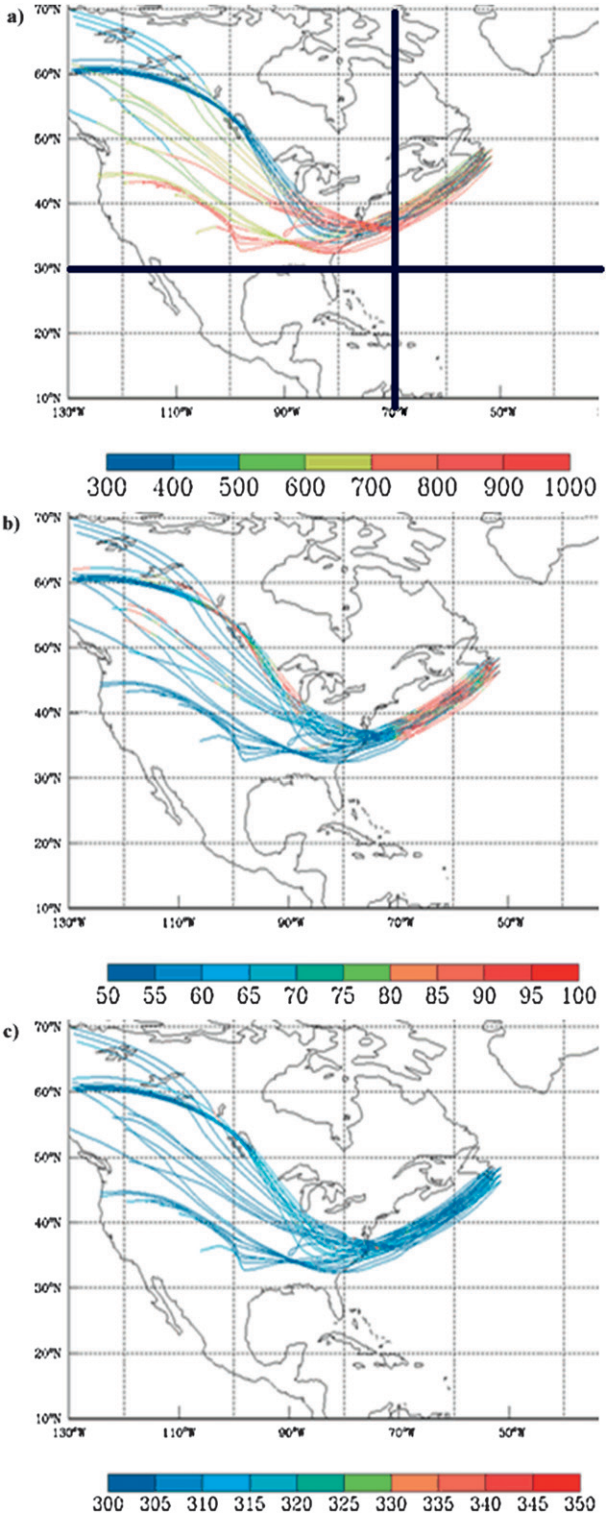

FIG. 4. As in Fig. 2, but for 0000 UTC 8 Dec 2000.

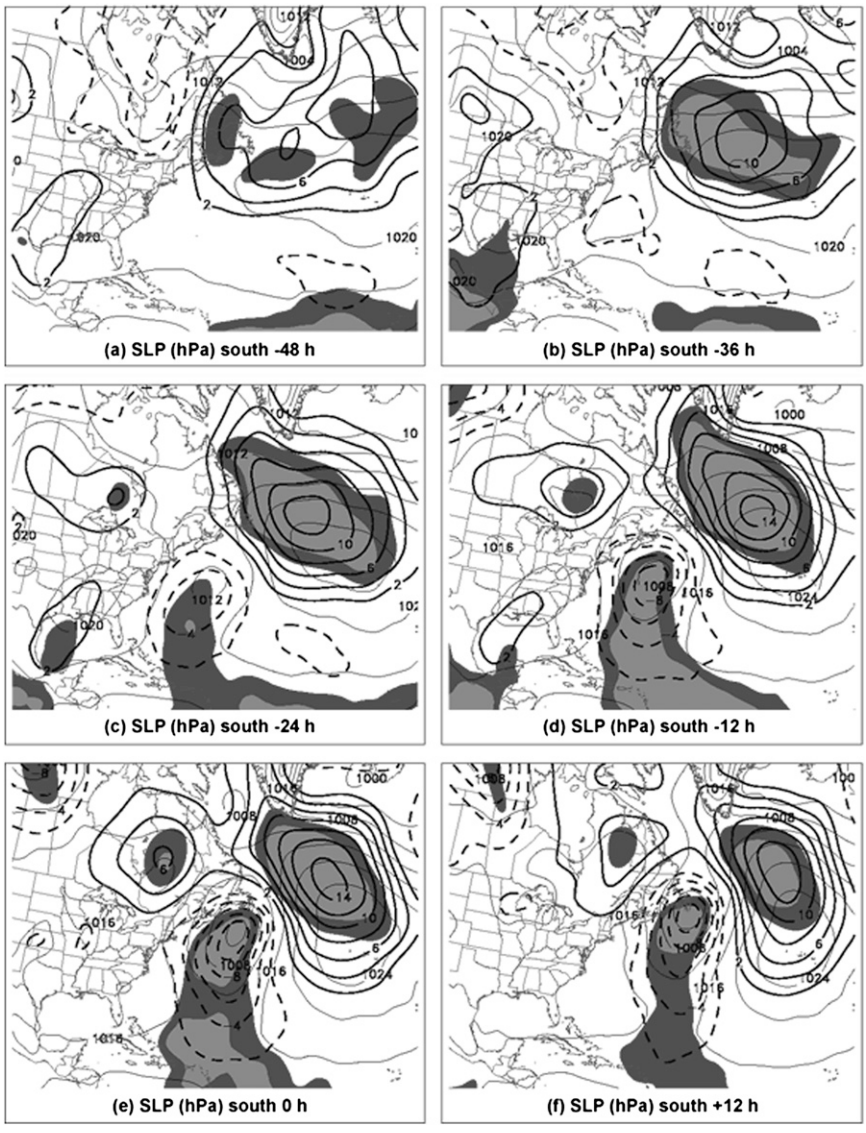

FIG. 5. SLP anomalies every 2 hPa, heavy dashed for negative values and heavy solid for positive values, with respect to climatology, for the south cases at (a) −48, (b) −36, (c) −24, (d) −12, (e) 0, and (f) +12 h. Light solid contours represent the full-composite SLP field, every 4 hPa. Shading represents the statistical significance of the anomalies at the 95% (darker shading) and 99% (lighter shading) confidence levels, according to the Student's *t* test.

trajectories extending 5 days backward. To be considered a south case, the starting points of the majority of the trajectories must be east of 70°W and thus originate completely from the Atlantic Ocean. The relative humidity of the air parcels (Fig. 2b) generally increases as the parcels approach $t = 0$ h and St. John's. Figure 2b shows that most of the air parcels are saturated or nearly saturated at the three ending levels in the vicinity of St. John's at $t = 0$ h. Finally, Fig. 2c depicts that for trajectories that did not interact with the boundary layer, values of the equivalent potential temperature (θ_e) remain relatively constant over the course of the 5-day evolution of the air parcel trajectories. The use of θ_e adds a level of objectivity to the partitioning of cases, as in a few cases the origin of the air parcels was slightly ambiguous and thus the event was classified by the location of the largest θ_e (Roberge et al. 2009).

Thirty-one cases are classified as southwest, including 0000 UTC 21 April 1988, shown in Fig. 3. To be classified as a southwest case, the majority of the trajectories must originate from south of 30°N and west of 70°W. This classification ensures that many of the trajectories in

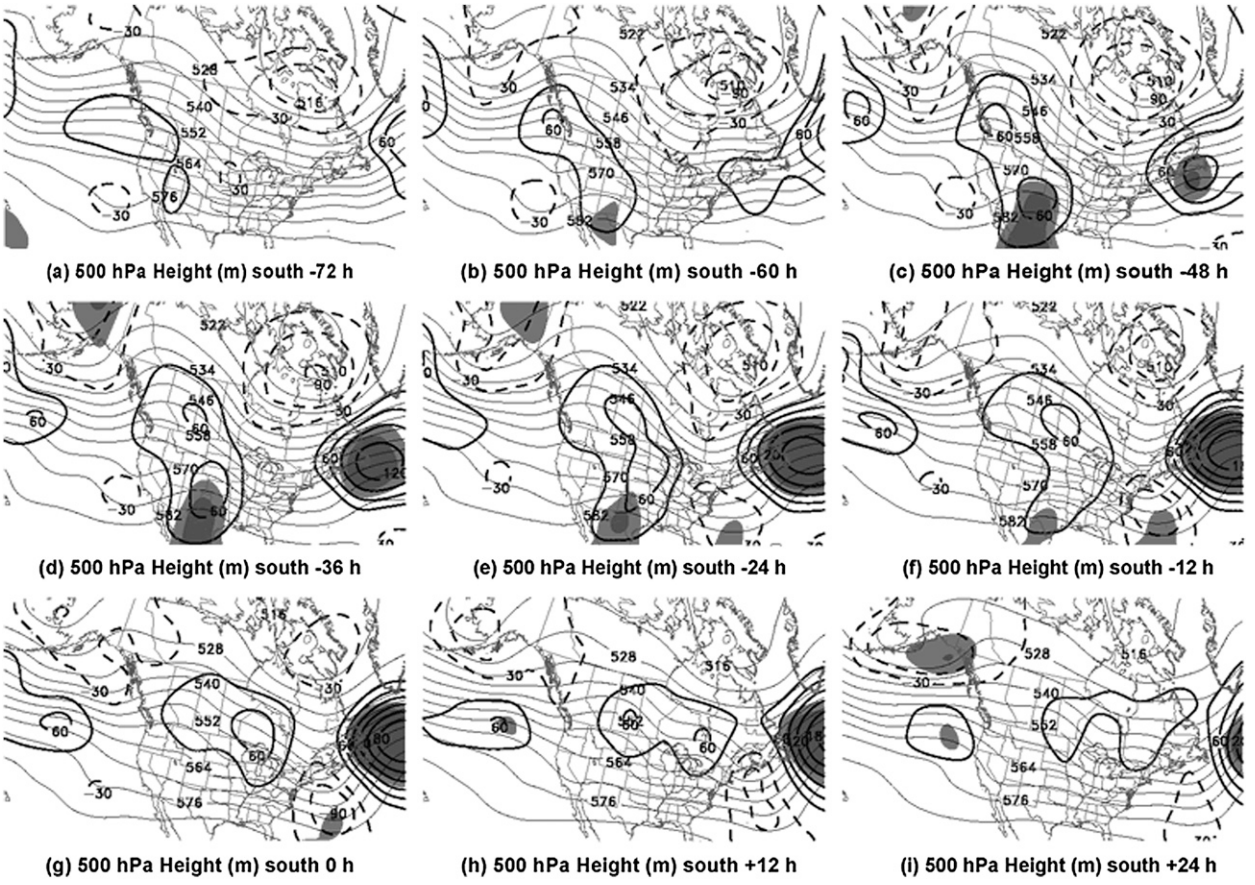

FIG. 6. The 500-hPa height anomalies, every 3 dam, with heavy dashed lines for negative values and heavy solid lines for positive values, with respect to climatology, for the composite of the south cases at (a) −72, (b) −60, (c) −48, (d) −36, (e) −24, (f) −12, (g) 0, (h) +12, and (i) +24 h. Light solid contours represent the full-composite 500-hPa field, every 6 dam. Shading represents the statistical significance of the anomalies at the 95% (lighter shading) and 99% (darker shading) confidence levels, according to the Student's *t* test.

a southwest case originate from the Gulf of Mexico (Fig. 3a). Additionally, Fig. 3b depicts that most of the trajectories are saturated or nearly saturated by $t = 0$ in the vicinity of St. John's.

Finally, eight cases are west cases, including Fig. 4, where $t = 0$ h is 0000 UTC 8 December 2000. West cases have trajectories that originate west of 70°W, but north of 30°N and thus north of the Gulf of Mexico. Therefore, most of the west cases have primarily continental source regions of air, as far back as 5 days (Fig. 4a). Finally, Fig. 4c differs from the south and southwest case examples in that the value of Θ_e is significantly lower, which is consistent with the continental origins of the parcels.

b. Composite results

Composite anomaly plots of three meteorological fields are displayed in order to understand the synoptic structures and precursors associated with each category of extreme event. Moreover, examining circulation anomalies in addition to the full composite fields allows the depiction of the significance of a particular feature with respect to a monthly weighted 30-yr (1971–2000) average. This process has been used many times, including by Grumm and Hart (2001). Some care should be taken when examining the statistical significance of the anomalies in the smaller groups, such as the west and south trajectory composites, although an examination of the individual cases within each composite shows high similarity among the synoptic structures. However, since the differences in synoptic structures among composite groups are so stark and make intuitive physical sense, this is not a major concern for the purpose of this paper. Finally, care should also be taken when directly comparing the strengths of the anomalies in any of the fields displayed in this paper; the monthly weighted climatological means are not always the same and thus may slightly skew the results. In general, a comparison of synoptic structures among different types should be done qualitatively rather than quantitatively.

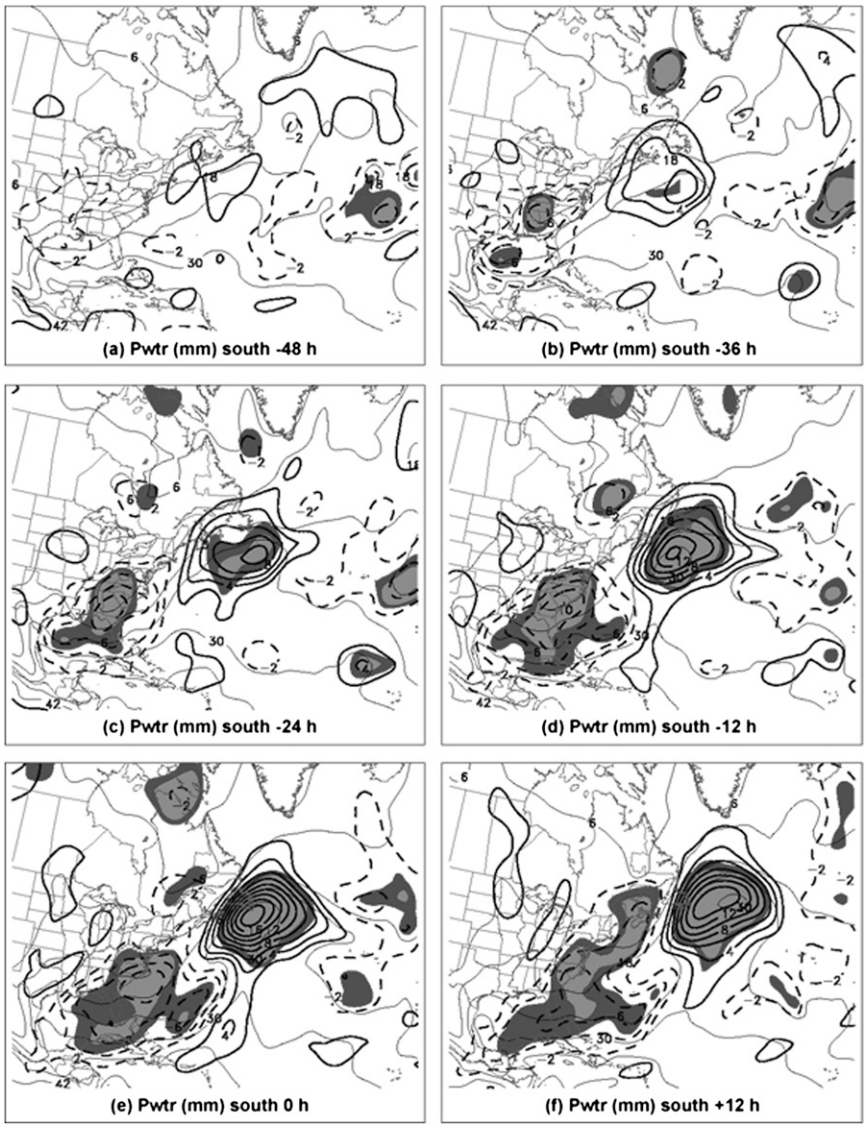

FIG. 7. PW anomalies every 2 mm, heavy dashed for negative values and heavy solid for positive values, with respect to climatology, for the south cases at (a) −48, (b) −36, (c) −24, (d) −12, (e) 0, and (f) +12 h. Light solid contours represent the full-composite PW field, every 6 mm. Shading represents the statistical significance of the anomalies at the 95% (lighter shading) and 99% (darker shading) confidence levels, according to the Student's *t* test.

Composite and anomaly plots of selected atmospheric mass fields are displayed every 12 h (these fields have been examined every 6 h, but due to space concerns are shown every 12 h) from $t = -48$ h to $t = +12$ h ($t = -72$ h to $t = +24$ h for the 500-hPa height anomaly plots), where $t = 0$ h is the time of onset of the heaviest precipitation at St. John's.

1) SOUTH TRAJECTORY COMPOSITES

In the south composite sea level pressure (SLP) field, a negative anomaly is not evident until $t = -24$ h (Fig. 5c). However, a positive anomaly is centered just downstream at $t = -48$ h (Fig. 5a), and is a precursor to an extreme south event at St. John's. The positive SLP anomaly east of St. John's is amplified from +8 hPa at $t = -48$ h (Fig. 5a) to +14 hPa at $t = -12$ h (Fig. 5d) just as the negative anomaly to the southwest is also amplified from −4 hPa at $t = -24$ h (Fig. 5c) to −10 hPa at $t = 0$ h (Fig. 5e). As discussed in Milrad et al. (2009), this is a possible indication that as the low pressure strengthens to the southwest of St. John's, both the warm air advection (WAA) and latent heat release (LHR) from precipitation

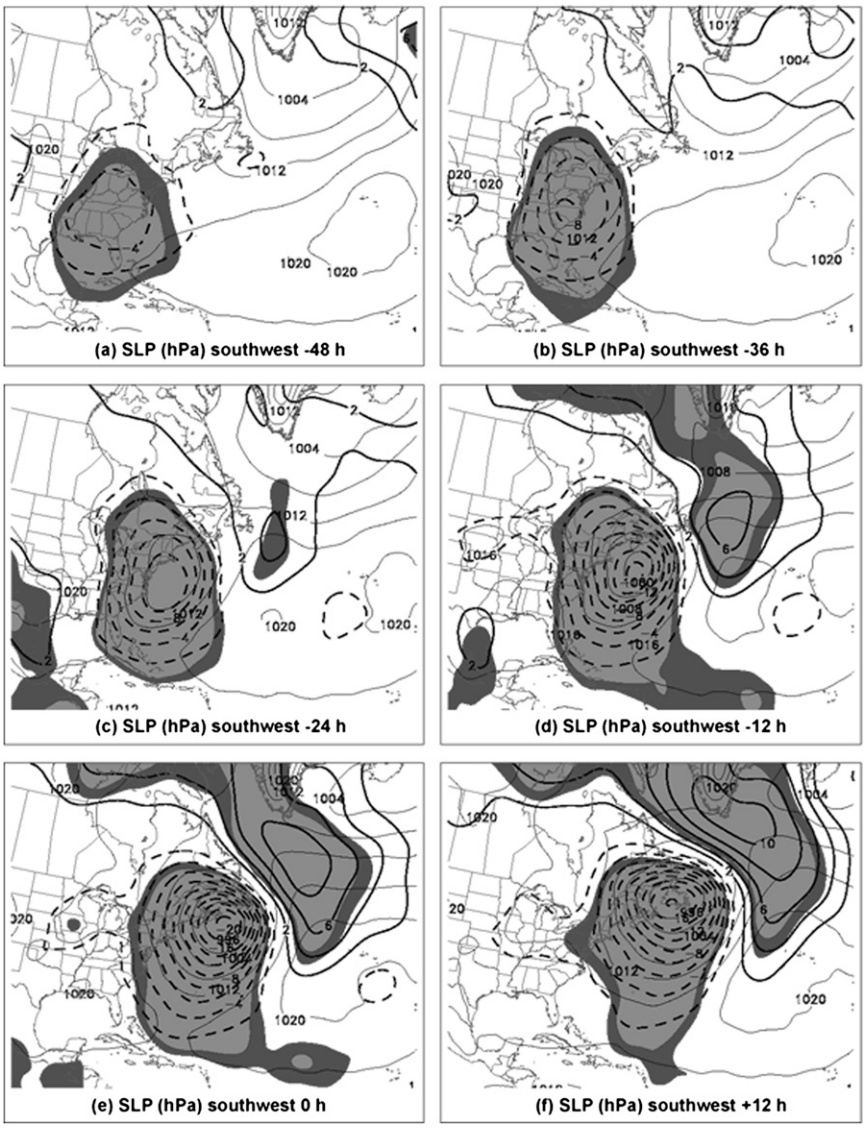

FIG. 8. As in Fig. 5, but for the southwest cases.

ahead of the low pressure system act to enhance the upper-level ridge (assuming both WAA and LHR increase with height above the surface), which in turn strengthens the surface high via anticyclonic vorticity advection. Although the WAA and LHR can have a competing effect of causing pressure/height falls at the surface near the surface high pressure (assuming colocation), the fact that the positive SLP anomaly strengthens during and shortly following the intensification of the upper-level ridge suggests that the vorticity advection aloft is sufficiently strong.

After $t = -12$ h (Fig. 5d), the mean and anomaly values of the anticyclone remain rather stagnant. The most notable difference between $t = -12$ h (Fig. 5d) and $t = 0$ h (Fig. 5e) is the translation of the mean anticyclone to the north, toward Greenland. This, in association with the SLP couplet oriented southwest to northeast, induces strong southerly geostrophic flow into St. John's ($t = -36$ to 0 h; Figs. 5b–e), suggesting moisture transport from the subtropical Atlantic. Finally, the sea level cyclone tracks just to the south and east of St. John's; this is an important point when comparing the south composite to the west and southwest composites.

In the 500-hPa height composite plot for the south cases (Fig. 6), an upper-level ridge associated with the surface anticyclone (Fig. 5a) is first observed directly south of St. John's at $t = -48$ h (Fig. 6c). At $t = -24$ h (Fig. 6e), the downstream ridge is now centered east-southeast of St. John's, with a magnitude of +150 m, having grown +90 m since $t = -48$ h (Fig. 6c). In

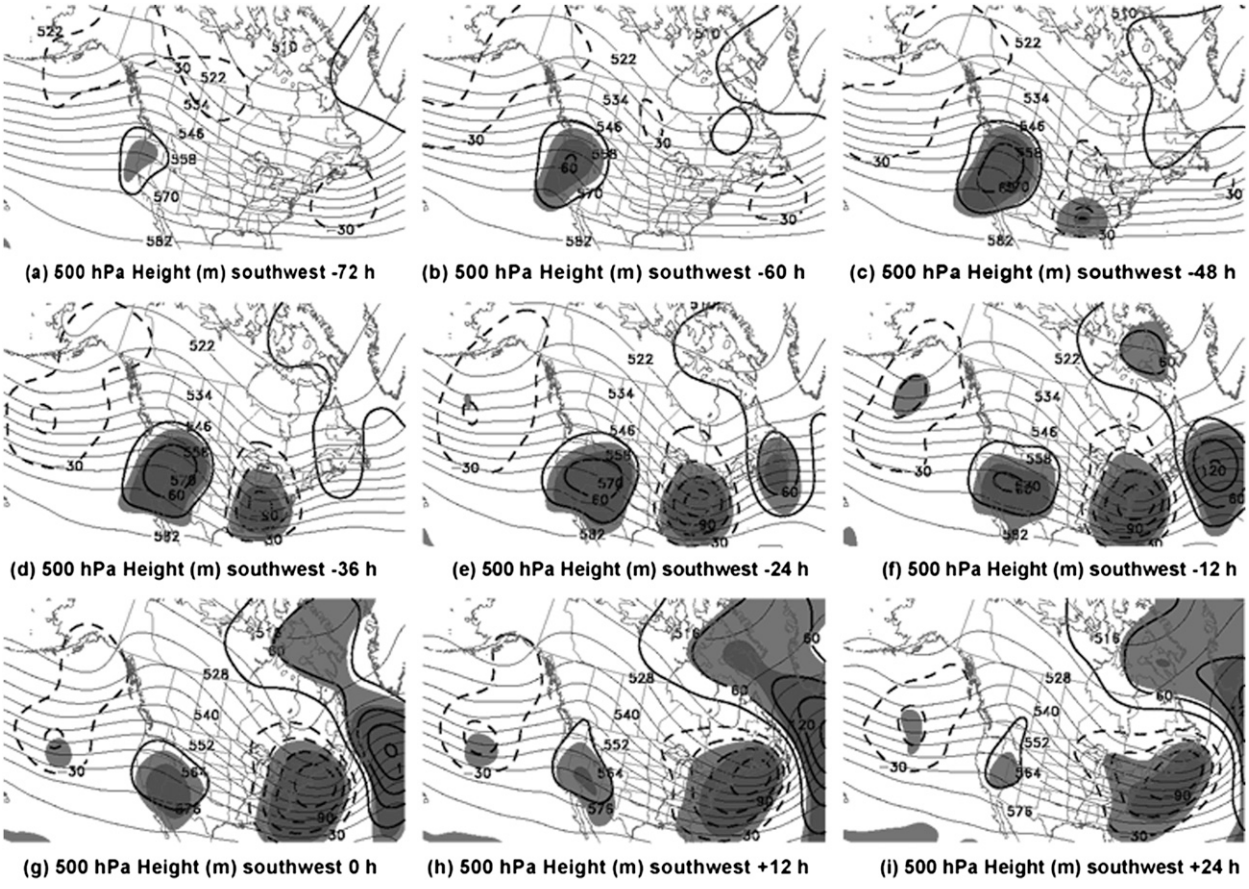

FIG. 9. As in Fig. 6, but for the southwest cases.

addition, a negative anomaly is first observed northeast of the Bahamas (Fig. 6e). As time moves forward to $t = 0$ h (Fig. 6g), this negative anomaly only strengthens slightly (−60 m), while the positive anomaly strengthens to more than +180 m.

The precipitable water (PW) composite field supports the assertion of strong moisture transport into St. John's, as a positive anomaly is first evident south of St. John's at $t = -36$ h (Fig. 7b). This anomaly moves eastward and amplifies as time progresses, reaching a maximum amplitude of +20 mm at $t = 0$ h (Fig. 7e), located just southeast of St. John's. Anomalously large values of PW are situated over St. John's by time $t = 0$ h.

2) SOUTHWEST TRAJECTORY COMPOSITES

The southwest composite SLP field is quite different from that of the south cases and resembles the overall extreme composite depicted in Milrad et al. (2009). This is not surprising given that 31 of the 50 extreme cases are in the southwest category. First, there is no evidence of a precursor downstream high pressure system east of St. John's. Instead, an anomalously strong cyclone is evident in the southeastern United States at $t = -48$ h (Fig. 8a). This area of low pressure strengthens and moves northeastward toward St. John's, reaching a minimum of −20 hPa at $t = 0$ h (Fig. 8e). An anomalously strong anticyclone starts to form at $t = -24$ h (Fig. 8c) to the east of St. John's and strengthens to an amplitude +10 hPa by $t = +12$ h (Fig. 8f). Overall, the key difference between the south and southwest composites is that the south cases are associated with an anomalously strong anticyclone downstream and the southwest cases are associated with both an anomalously strong cyclone upstream and anomalously strong anticyclone downstream, albeit one that forms at a later time than the anticyclone in the south composite. Geostrophically, the winds at St. John's at $t = 0$ are southeasterly, again bringing moisture from the Atlantic Ocean. The negative SLP anomaly in the southwest cases tracks just to the west of St. John's, suggesting that at least some of the rainfall occurs in association with a warm front ahead of the surface cyclone.

As seen in Milrad et al. (2009) for the overall extreme composite, a precursor ridge is observed at $t = -72$ h in

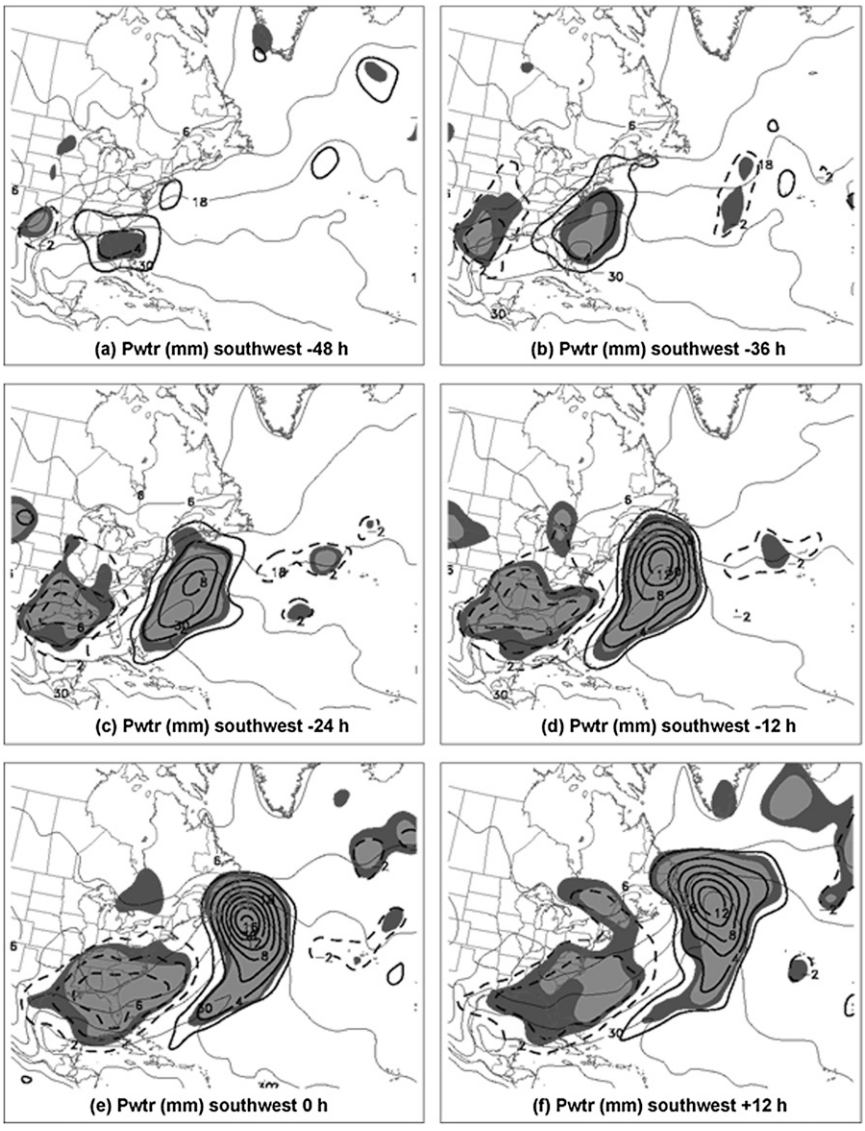

FIG. 10. As in Fig. 7, but for the southwest cases.

the Pacific Northwest region of the United States (Fig. 9a). This anomaly grows in amplitude and slowly slides eastward by $t = -48$ h (Fig. 9c), when a negative anomaly downstream of the initial positive anomaly is first observed. Over the subsequent 24–36 h, the original upstream positive height anomaly slowly weakens as the negative anomaly grows in strength (-90 m at $t = -24$ h; Fig. 9e). In addition, a new downstream positive anomaly forms at $t = -24$ h just south of St. John's (Fig. 9e). As the negative anomaly maintains its intensity (or slightly weakens) from $t = -12$ h through $t = +24$ h, the downstream positive anomaly grows in amplitude (Figs. 9f–i).

The southwest composite depicts a positive PW anomaly at $t = -48$ h (Fig. 10a) located in the northeastern Gulf of Mexico. This anomaly propagates northeastward toward St. John's while intensifying from +4 mm at $t = -48$ h (Fig. 10a) to +16 mm at $t = 0$ h (Fig. 10e). The spatial scale of the positive anomaly near St. John's at $t = 0$ h (Fig. 10e) is very similar to the south composite, with the differences being the formation region and the path traveled to St. John's.

3) WEST TRAJECTORY COMPOSITES

The west composite is notable for the lack of an anomalously strong downstream positive SLP anomaly during the 60-h evolution shown in Fig. 11. An upstream negative anomaly is first visible at $t = -36$ h (Fig. 11b) in the Great Lakes region, much farther to the north and

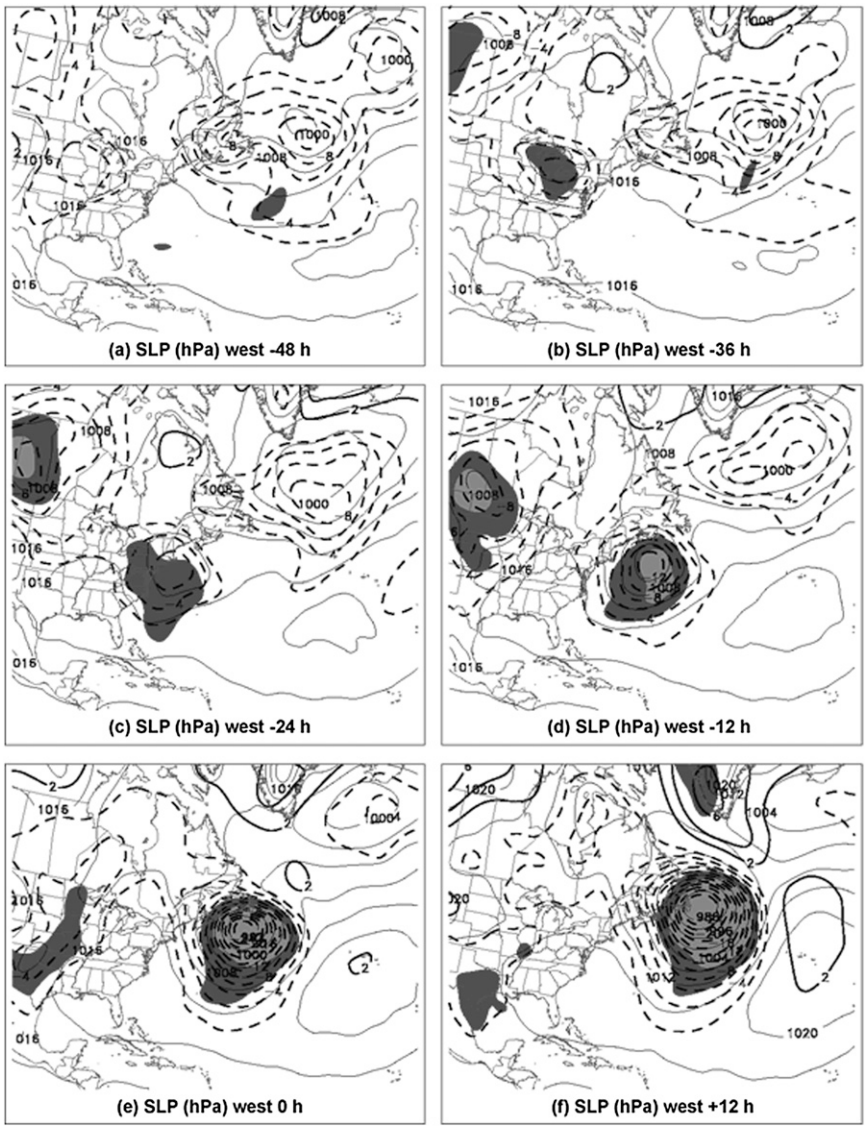

FIG. 11. As in Fig. 5, but for the west cases.

west than in the south and southwest cases. The negative anomaly does not intensify until it reaches the warm, lower static stability air over the Gulf Stream by $t = -12$ h (Fig. 11d). The intensification rate of the composite negative anomaly between $t = -24$ h (Fig. 11c) and $t = 0$ h (Fig. 11e) is 22+ hPa over the course of 12 h. For a west case to be an extreme event, an Alberta clipper–type system has to rapidly develop once it moves over the western Atlantic. Unlike in the southwest cases, the center of the negative SLP anomaly passes just to the south and east of St. John's.

The 500-hPa height composite field in the west cases (Fig. 12) depicts a system that initially has weak upper-level support, which increases once the low-level cyclone center starts to intensify over the ocean. A weak negative anomaly is visible at $t = -36$ h over the Great Lakes region (Fig. 12d) and approaches St. John's from the south at $t = 0$ h (Fig. 12g). The suggestion here is that baroclinic instability is present, as the near-surface cyclone helps to intensify the upstream upper-level trough by advecting cold air beneath 500 hPa (not shown) into the base of the 500-hPa trough. In examining Figs. 12f–h, the 500-hPa negative height anomaly intensifies from -120 m at $t = -12$ h to -210 m at $t = +12$ h. The enhancement of the upper-level trough via cold-air advection creates a positive feedback loop whereby the differential cyclonic vorticity advection (not shown) associated with the 500-hPa trough indirectly intensifies

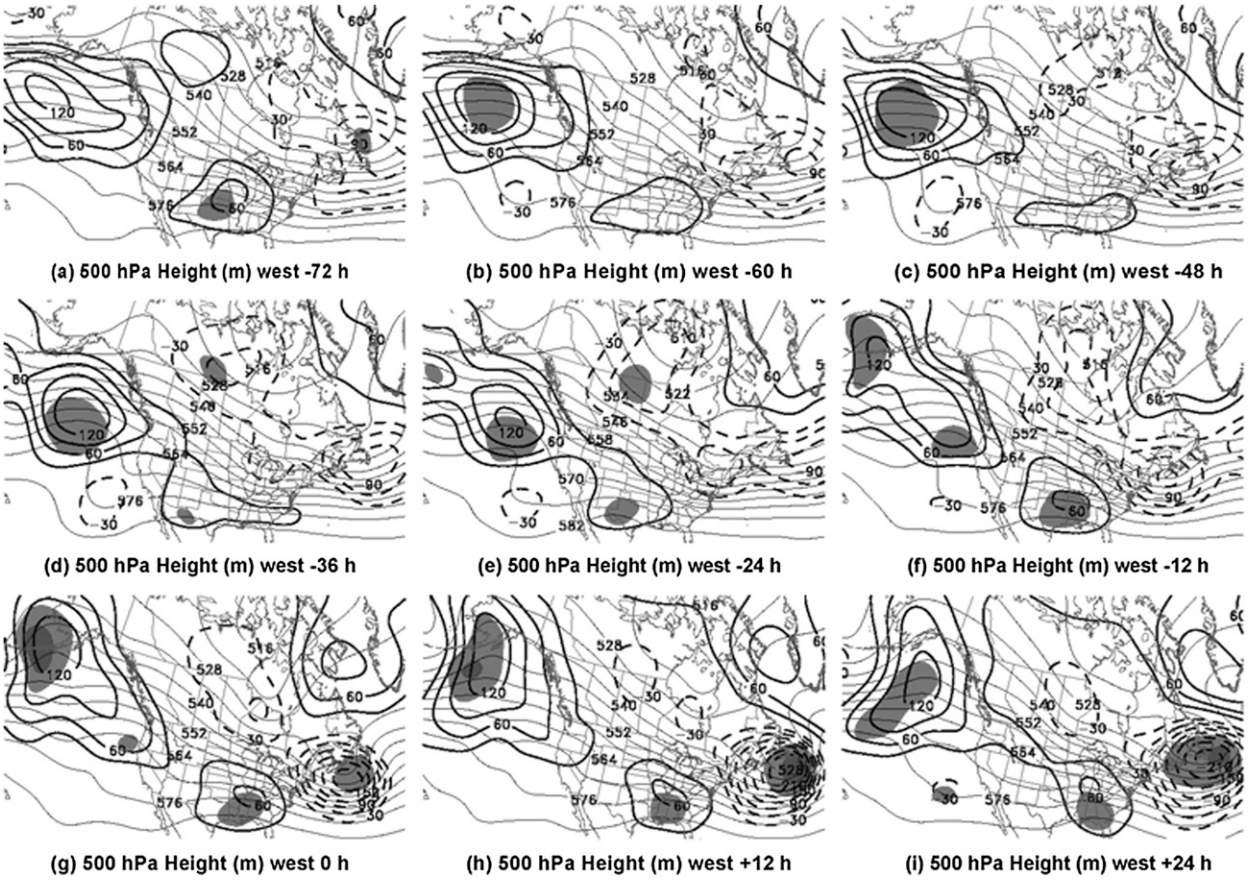

FIG. 12. As in Fig. 6, but for the west cases.

the surface cyclone, which then acts to intensify the upper-level trough through stronger low-level cold-air advection.

Evident in Fig. 13a are two precursor anomalies: a negative PW anomaly centered just southeast of St. John's at $t = -48$ h and a positive anomaly centered over the central United States. While the positive anomaly is not statistically significant, the authors believe this is mostly due to a low number of cases in the west composite (eight cases) and that the structure and location of this anomaly are still important. As time moves forward, the positive PW anomaly over the central plains of the United States splits into two anomalies, with one remaining over the area by $t = -12$ h (Fig. 13d) and the other moving eastward off the east coast, where it intensifies by $t = -12$ h (Fig. 13d). The positive anomaly over the plains is likely in association with the strong Alberta clipper over the Great Lakes, which pulls warm, moist air northward from the Gulf of Mexico. This positive anomaly subsequently continues north-northeastward until it is centered just south of St. John's at $t = 0$ h (Fig. 13e).

4. Synoptic typing II: Using quasigeostrophic forcing parameters

a. Partitioning methodology

The second method of event parsing involves 1000–700-hPa horizontal temperature advection, 700–400-hPa vorticity advection, and 1000–700-hPa geostrophic frontogenesis. Time series of these three parameters are plotted for a sample case of each category of extreme event in Fig. 14a (cyclone) and Fig. 14b (frontal). Values are based on a weighted average of the values at the three nearest grid points to the station of interest.

Figure 14a displays the time series of an example of the cyclone group from 30 December 1997. The evolution of the three parameters is typical for the passage of a midlatitude extratropical cyclone. The values of the low-level warm-air advection and frontogenesis are relatively high during the first part of the time series, coinciding with the likely passage of the warm front ahead of the main surface cyclone. In subsequent time periods, values of horizontal temperature advection become negative as the main upper-level trough approaches

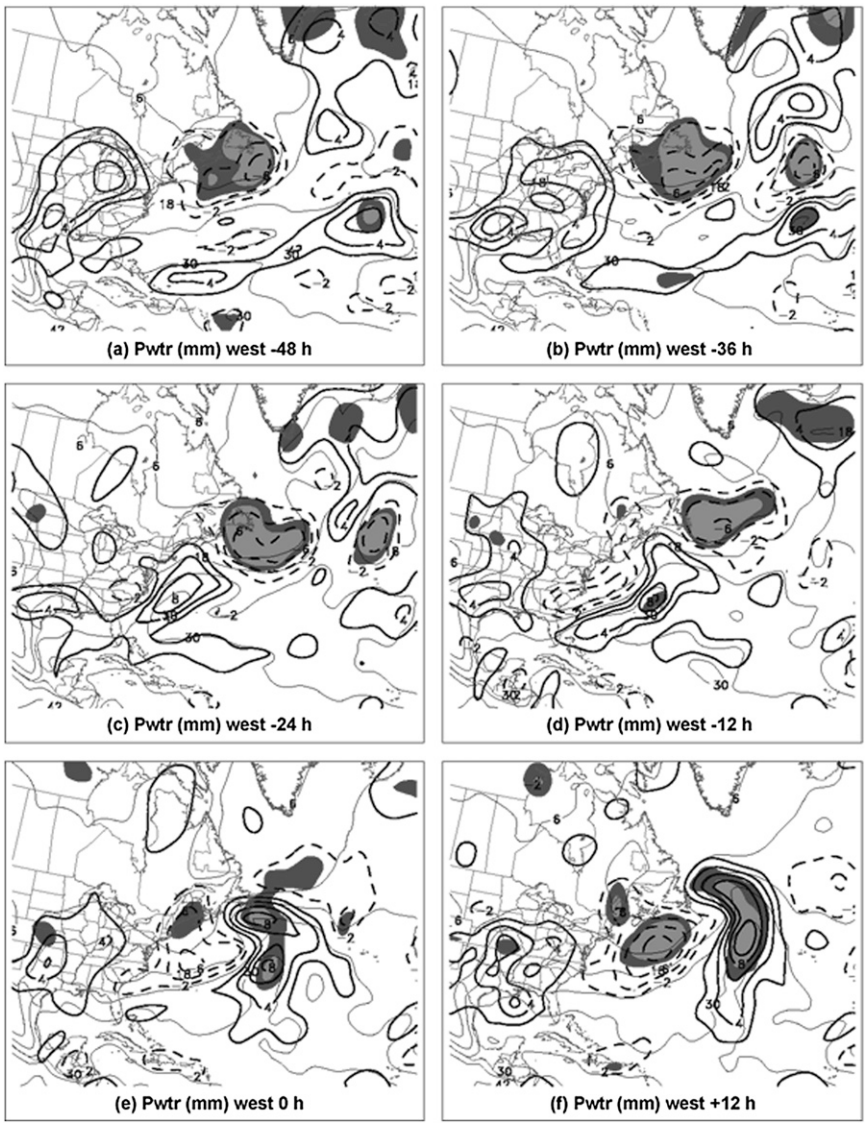

FIG. 13. As in Fig. 7, but for the west cases.

and passes St. John's. Concomitantly, the values of the midtropospheric vorticity advection go from near zero to positive values as the upstream upper-level trough approaches St. John's. In all of the 35 cyclone cases, the 1000–700-hPa layer-averaged frontogenesis is less than 20×10^{-2} K (100 m)$^{-1}$ (3 h)$^{-1}$ on average during the $t = -12$ h to $t = +12$ h time frame. Moreover, the evolution of the three QG forcing parameters described above is evident for the vast majority of cyclone cases (27 of 35). The remainder of the cyclone cases differs in that the values of the 700–400-hPa layer-averaged vorticity advection are lower than the other 27 cyclone cases during the time frame discussed, with low-level warm-air advection dominating. These eight events are characterized by an intense sea level cyclone that tracks well west of St. John's, placing the station in a broad area of warm-air advection, and by an upper-level trough that moved sufficiently west of St. John's such that values of midlevel vorticity advection at the station are significantly weaker than the other 27 cyclone cases. While it is arguable that the cyclone group could be broken down into two subgroups, a main goal of this paper is to isolate the synoptic structures associated with extreme precipitation events in which a strong sea level cyclone is not present (i.e., the frontal group) and compare them with structures during events in which a strong sea level cyclone is present (cyclone group).

Figure 14b displays an example of the frontal group from 5 February 1984. Both the horizontal temperature advection and midlevel vorticity advection values are

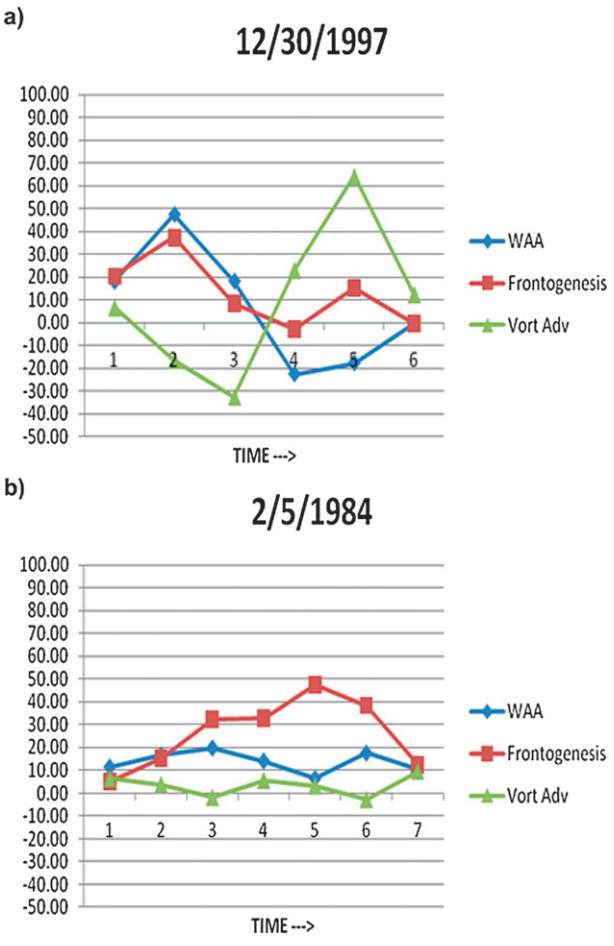

FIG. 14. Time series—during which precipitation was recorded at St. John's—of NCEP–NCAR reanalysis 700–400-hPa layer-averaged relative vorticity advection ($\times 10^{-10}$ s^{-1}; green), 1000–700-hPa layer-averaged horizontal temperature advection ($\times 10^{-5}$ K s^{-1}; blue), and 1000–700-hPa layer-averaged frontogenesis [$\times 10^{-2}$ K (100 m)$^{-1}$ (3 h)$^{-1}$; red] for (a) a cyclone case and (b) a frontal case.

near zero during the event. However, the value of the 1000–700-hPa geostrophic frontogenesis is consistently large throughout the event. The evolution of the three QG forcing parameters is examined during the period from 12 h prior ($t = -12$ h) to 12 h after ($t = +12$ h) the onset of the heaviest precipitation at St. John's. The criteria for frontal events are as follows:

- 1000–700-hPa layer-averaged geostrophic frontogenesis, $\geq 30 \times 10^{-2}$ K (100 m)$^{-1}$ (3 h)$^{-1}$;
- 1000–700-hPa layer-averaged temperature advection, $\leq 20 \times 10^{-5}$ K s^{-1}; and
- 400–700-hPa layer-averaged vorticity advection, $\leq 10 \times 10^{-10}$ s^{-1}.

While these values may appear arbitrary, all 11 frontal cases fit these criteria extremely well, while no other cases come close to doing so.

The 1000–700-hPa frontogenesis is chosen for use in this paper primarily because it is a commonly examined variable operationally and is useful in pinpointing the location of low-level temperature gradients, which serve as the primary mechanism for quasigeostrophic ascent.

Finally, results for the cases in this study show that in the frontal cases, the magnitude of the normal component of frontogenesis (for which $\mathbf{Q}_n$ is used as a proxy, as defined in section 2a) is greater than that of the parallel component (for which $\mathbf{Q}_s$ is used as a proxy, as defined in section 2a), while the opposite is true in most of the cyclone cases (not shown). In the remaining cyclone cases, the magnitudes of both components are near zero. The observed evolution of the two components of frontogenesis further supports the partitioning methodology outlined in this section. The frontogenesis components in the frontal cases suggest that as time passes, the focus of the frontogenesis moves from the synoptic scale to the mesoscale, as found by Gyakum and Barker (1988). A caveat to this point is that real wind frontogenesis, not geostrophic frontogenesis, more accurately represents what is happening in mesoscale frontal circulations. While this is beyond the scope of this paper, the time evolutions of the 1000–700-hPa layer-averaged geostrophic frontogenesis and 1000–700-hPa layer-averaged frontogenesis derived from the real wind are similar for all of the cases in this paper (not shown).

In total, there are 35 cases classified in the cyclone group and 11 cases classified in the frontal group.

b. Composite results

1) CYCLONE COMPOSITES

In the SLP field, an anomalously strong cyclone is visible at $t = -48$ h (Fig. 15a) over northern Florida. This anomaly moves northeastward and rapidly strengthens, reaching an amplitude of -10 hPa at $t = -24$ h (Fig. 15c) and -20 hPa at $t = 0$ h, when the cyclone center is located just southwest of St. John's. Although there is a positive anomaly downstream starting at $t = -48$ h (Fig. 15a), the amplitude of this feature over time (Figs. 15a–f) remains relatively weak until $t = 0$ and $+12$ h.

A precursor positive 500-hPa height anomaly is evident along the west coast of the United States at 3 days ($t = -72$ h) prior (Fig. 16a) to the onset of the heaviest precipitation at St. John's. The positive anomaly grows in size until around $t = -36$ h (Fig. 16d), after which it slowly begins to weaken. Additionally, a negative height anomaly downstream of the initial positive anomaly is first evident at $t = -36$ h (Fig. 16d) and grows in size and amplitude to a maximum intensity of -150 m at $t = 0$ h

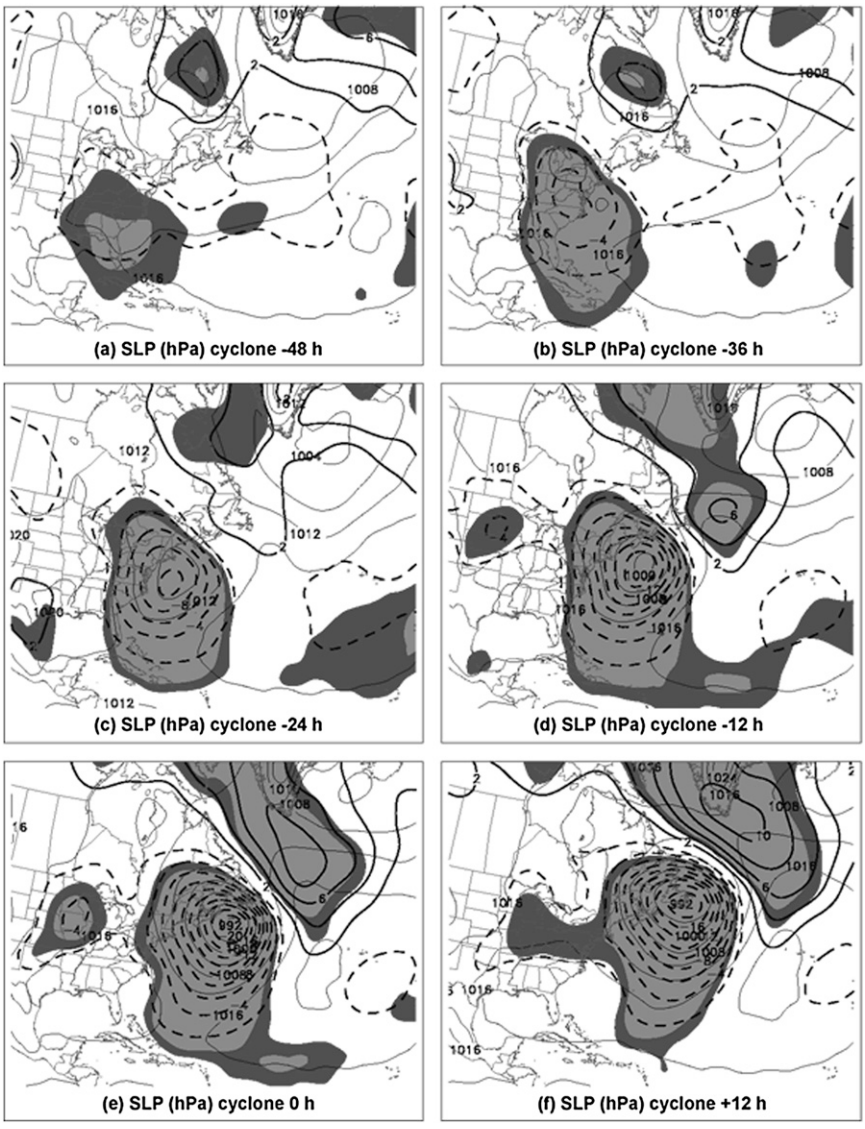

FIG. 15. As in Fig. 5, but for the cyclone cases.

(Fig. 16g) and $t = +12$ h (Fig. 16h). The fact that the negative anomaly steadily strengthens as the upstream positive anomaly weakens is supportive of the downstream Rossby wave development discussed in Milrad et al. (2009). This is also supported by the development of a second positive anomaly downstream of the negative anomaly, first evident at $t = -12$ h (Fig. 16f) just east of St. John's. This downstream negative anomaly grows in amplitude through $t = 0$ h (Fig. 16g) and beyond.

A positive PW anomaly is evident just off the southeastern coast of the United States at $t = -36$ h (Fig. 17b). This anomaly strengthens and moves northeastward toward St. John's, reaching a maximum intensity of +14 mm at $t = 0$ h (Fig. 17e).

2) FRONTAL COMPOSITES

In the SLP field, a strong downstream high pressure system (positive anomaly) is located east of St. John's at $t = -48$ h (Fig. 18a). This positive anomaly grows in amplitude and reaches a maximum of +14 hPa at $t = -24$ h (Fig. 18c). It helps to initiate moist southerly flow off the Atlantic Ocean and into St. John's. Concomitantly, a weak negative SLP anomaly moves eastward from the Great Lakes region at $t = -48$ h (Fig. 18a) and redevelops to the southeast once it reaches the Atlantic Ocean at $t = -12$ h (Fig. 18d). This weak negative anomaly then propagates northeastward until it is located just southwest of St. John's at $t = 0$ h (Fig. 18e), by which time it has an amplitude of −8 hPa, compared

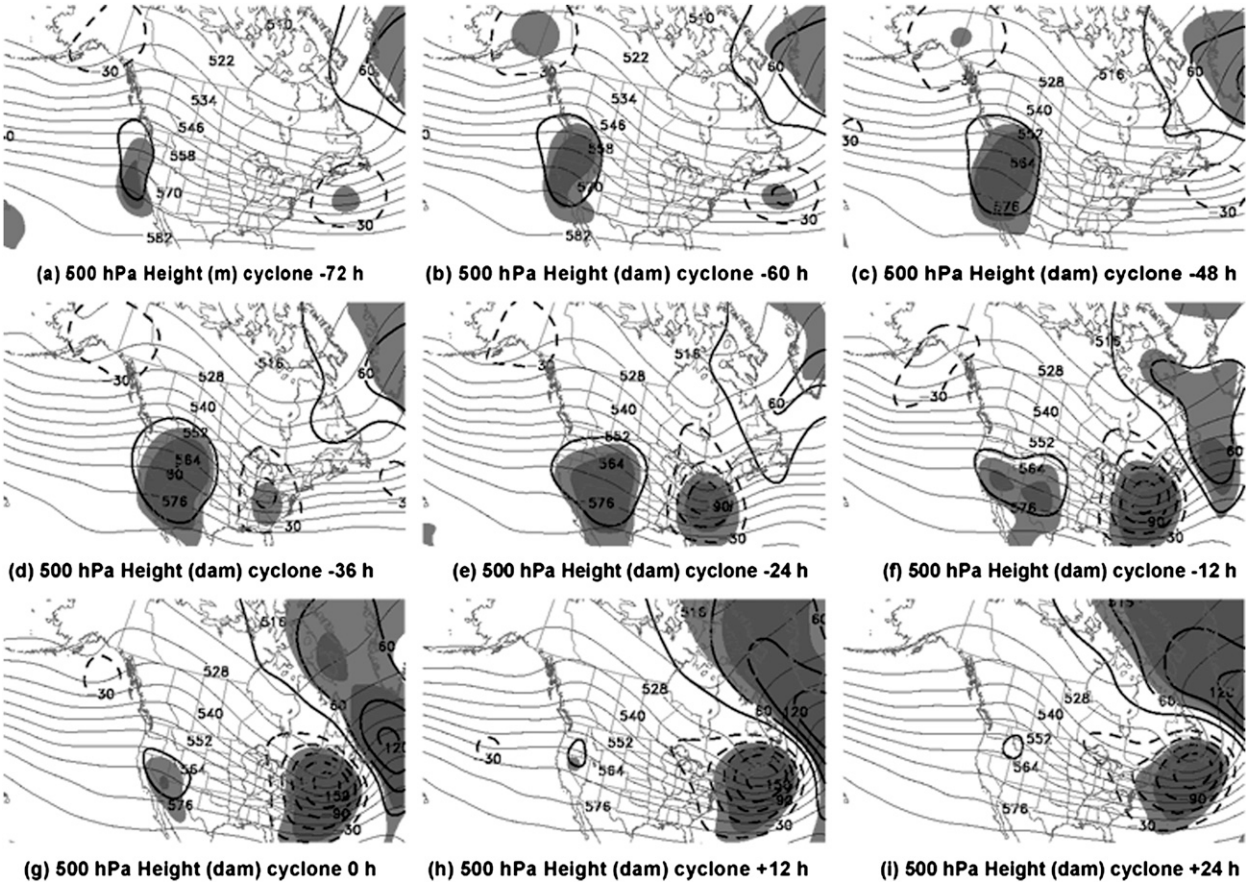

FIG. 16. As in Fig. 6, but for the cyclone cases.

with −20 hPa in the cyclone composite. The emergence of a new anomaly to the southeast between $t = -24$ h (Fig. 18c) and $t = -12$ h (Fig. 18d) suggests that as the original cyclone moves eastward from the Great Lakes, a second wave of low pressure develops along a quasi-stationary baroclinic zone that is established to the west of the downstream high pressure system and along the eastern seaboard.

In the 500-hPa height composite, a downstream 500-hPa ridge is evident (Fig. 19) and remains quasi-stationary during the period of precipitation at St. John's, supporting the presence of a downstream surface anticyclone. Meanwhile, a weak upstream trough is present from $t = -72$ h (Fig. 19a) to $t = +24$ h (Fig. 19i).

A positive PW anomaly is first evident at $t = -36$ h (Fig. 20b), centered just southwest of St. John's. This anomaly proceeds to strengthen and slowly move eastward through $t = 0$ h (Fig. 20e), when it reaches a maximum intensity of +16 mm centered just southeast of St. John's. In contrast to the cyclone group, the positive PW anomaly in the frontal group is relatively stationary, in accordance with the suggestion that a quasi-stationary deformation zone is situated upstream of the sea level anticyclone, right over St. John's. The PW anomaly finally starts to move eastward as the weak wave of low pressure moves northeastward along the stationary front, bringing the heaviest of the precipitation into St. John's by $t = 0$ h (Fig. 20e).

5. Concluding discussion and future work

This study takes a closer look at the 50 median extreme precipitation events identified in Milrad et al. (2009). Two manual classification schemes are utilized to explore their associated synoptic structures. The first methodology involves a 5-day backward-trajectory analysis, out of which three groups of extreme events are defined based on the origin of the majority of their air parcels. These groups are defined as south (11 events), southwest (31 events), and west (8 events). The second methodology revolves around a time series analysis of three QG ascent-forcing parameters. Forty-six of the 50 events are subsequently classified into cyclone (35 events) and frontal (11 events) groups.

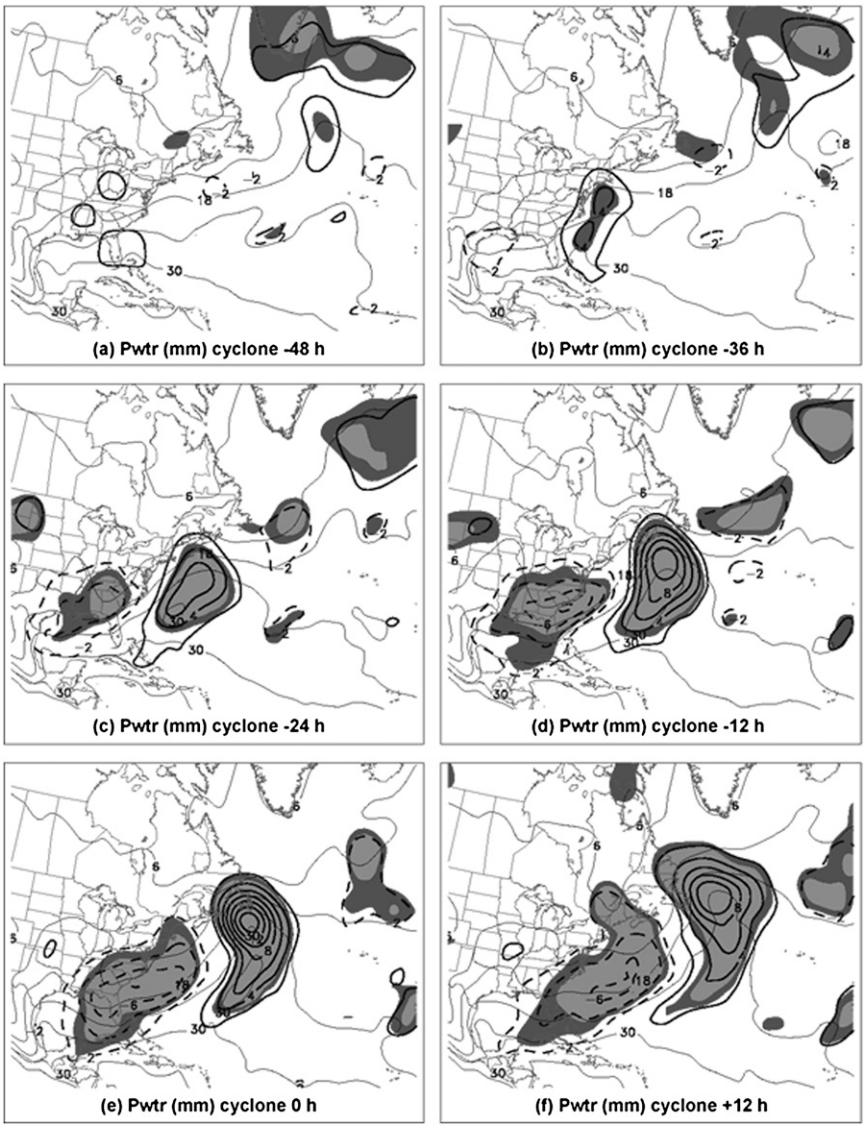

FIG. 17. As in Fig. 7, but for the cyclone cases.

In the south cases, the pattern is dominated by a downstream surface anticyclone and corresponding mid-tropospheric ridge (Fig. 5). This southerly flow helps to transport moisture and create a positive PW anomaly just south of St. John's at $t = -24$ h (Fig. 7c). Subsequently, the PW anomaly amplifies and propagates toward St. John's. In turn, the downstream ridge is amplified by both warm-air advection ahead of the low-level cyclone and latent heat release from heavy precipitation, as discussed in Milrad et al. (2009); once the downstream ridge has amplified, the surface anticyclone amplifies in response to enhanced anticyclonic vorticity advection above the surface anticyclone center.

The southwest trajectory cases are pointedly similar to that of the overall extreme composite presented in Milrad et al. (2009). In the southwest composite, an anomalous sea level cyclone forms near the northeastern Gulf of Mexico at around $t = -72$ h (not shown) and slowly amplifies as it progresses northeastward. By time $t = -12$ h (Fig. 8d), a downstream anticyclone begins to form just east of St. John's. It is suggested that two processes are at play: 1) downstream development associated with Rossby wave energy transfer and 2) enhancement of the downstream ridge due to warm-air advection and latent heat release ahead of the surface cyclone, which in turn strengthens the surface anticyclone via differential anticyclonic vorticity advection.

Corresponding to the first point, a precursor 500-hPa height ridge is evident over the western United States

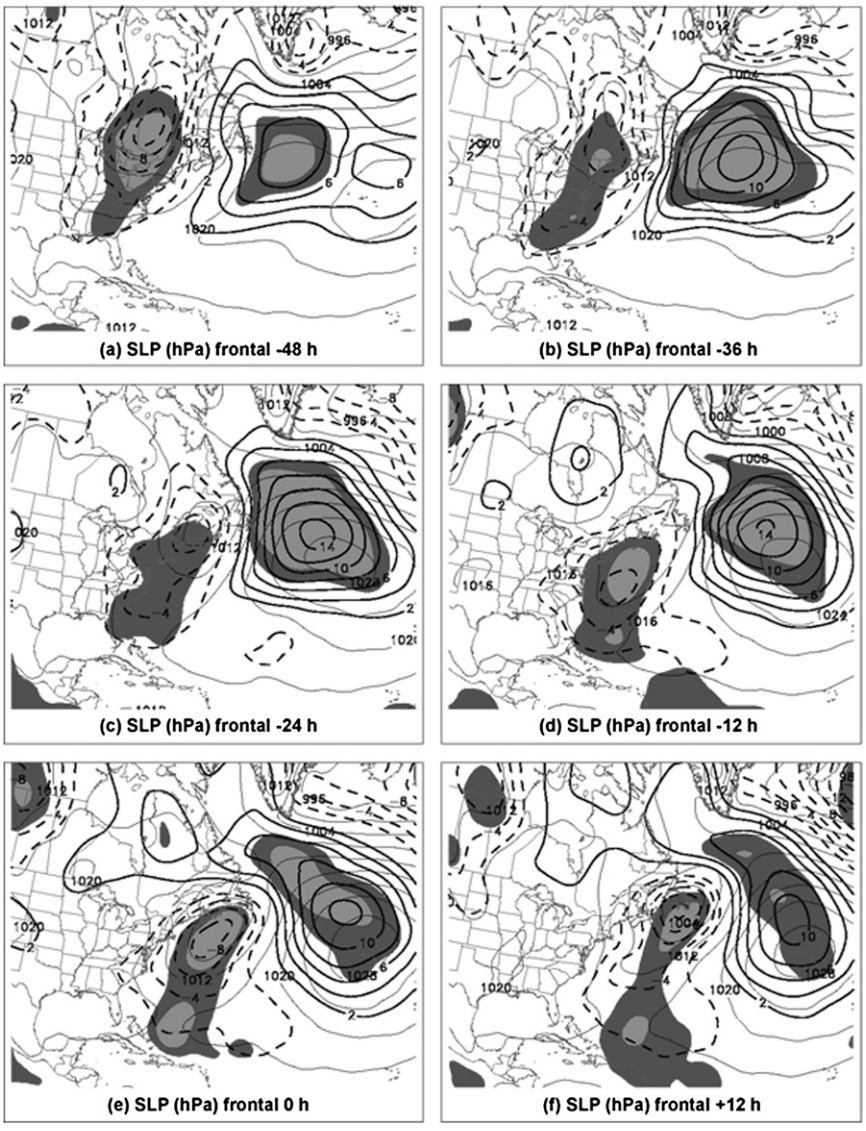

FIG. 18. As in Fig. 15, but for the frontal cases.

at 3 days ($t = -72$ h) prior to the onset of heaviest precipitation at St. John's. This positive anomaly first amplifies, then subsequently weakens around $t = -36$ h (Figs. 9a–i), as the downstream negative anomaly starts to amplify. The trough initially amplifies, then approximately maintains its intensity while a downstream ridge amplifies east of St. John's. This downstream development is not evident in the south or west cases. Finally, the positive PW anomaly is more transient in the southwest cases than in the south cases, forming over northern Florida (Fig. 10a) at $t = -48$ h and moving northeastward toward St. John's while intensifying.

The west trajectory cases feature synoptic structures that are markedly different from both the south and southwest cases. In the SLP composite field, a weak cyclone emerges from the Great Lakes region around $t = -24$ h (Fig. 11c) and rapidly intensifies upon reaching the Atlantic Ocean. In the 500-hPa height field, the negative anomaly (trough) associated with the surface cyclone also rapidly intensifies upon reaching the Atlantic Ocean. The amplitude of the 500-hPa trough suggests that the overall dynamics of the west cases are relatively strong, but there is a lack of low-level baroclinicity and relatively high static stability while the system is over the continent. Upon reaching the Atlantic Ocean (i.e., a moisture source with overlying lower static stability air), the near-surface cyclone rapidly intensifies, which further intensifies the upper-level trough. As time progresses, these systems continue to rapidly intensify each other via baroclinic instability.

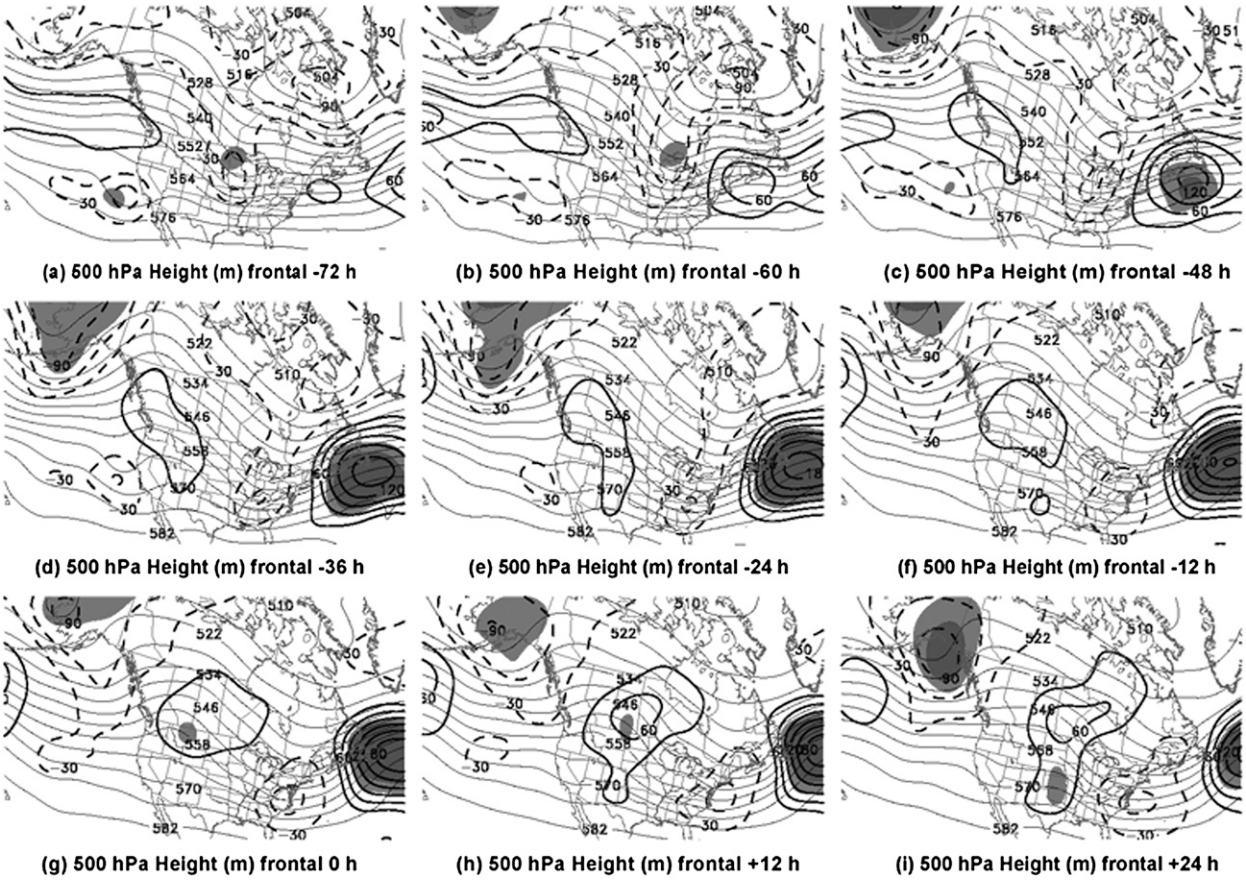

FIG. 19. As in Fig. 16, but for the frontal cases.

While the Atlantic Ocean clearly plays an important role in providing enough moisture for a west case to be an extreme event, the PW composite for the west cases suggests that a potential precursor signal to these events is located in the Great Plains of the United States. A positive PW anomaly is present over the Great Plains at $t = -48$ h (Fig. 13a), 2 days before the onset of the heaviest precipitation at St. John's. While a piece of this anomaly remains relatively stationary over time, another piece propagates eastward, reaching the Atlantic Ocean at the same time ($t = -24$, Fig. 13c) that the sea level cyclone begins to rapidly intensify off the east coast of the United States. This positive PW anomaly subsequently moves northeastward toward St. John's in conjunction with the surface cyclone. It is of note that both the strength of the 500-hPa trough and the track of the sea level cyclone in the west trajectory composite in this paper are similar to those seen in the light precipitation event composite shown in Milrad et al. (2009). Thus, the light cases in Milrad et al. (2009) may serve as null cases to the extreme west cases described in this paper.

The second manual classification methodology produces two groups of cases, deemed cyclone (35 cases) and frontal (11 cases). The synoptic signals in the frontal group are masked by the cyclone group in the overall extreme composite discussed in Milrad et al. (2009).

In the cyclone composite, negative SLP and positive PW anomalies form concurrently over northern Florida at $t = -48$ h (Figs. 15a and 17a). These anomalies proceed to strengthen and move northeastward toward St. John's, reaching a maximum amplitude by $t = 0$ h (Figs. 15e and 17e). Meanwhile, the downstream SLP anomaly is relatively weak compared with the frontal composite. The same processes involved in strengthening the downstream anomalies in the southwest and overall extreme composite are at work in the cyclone composite. To that end, a positive 500-hPa precursor height anomaly is visible over the west coast of the United States at $t = -72$ h (Fig. 16a). Finally, soundings produced for $t = -12$ h to $t = +12$ h at St. John's (not shown) depict a strong 1000–700-hPa veering wind signal, which supports the assertion of strong low-level warm-air advection as the cyclone passes St. John's. The

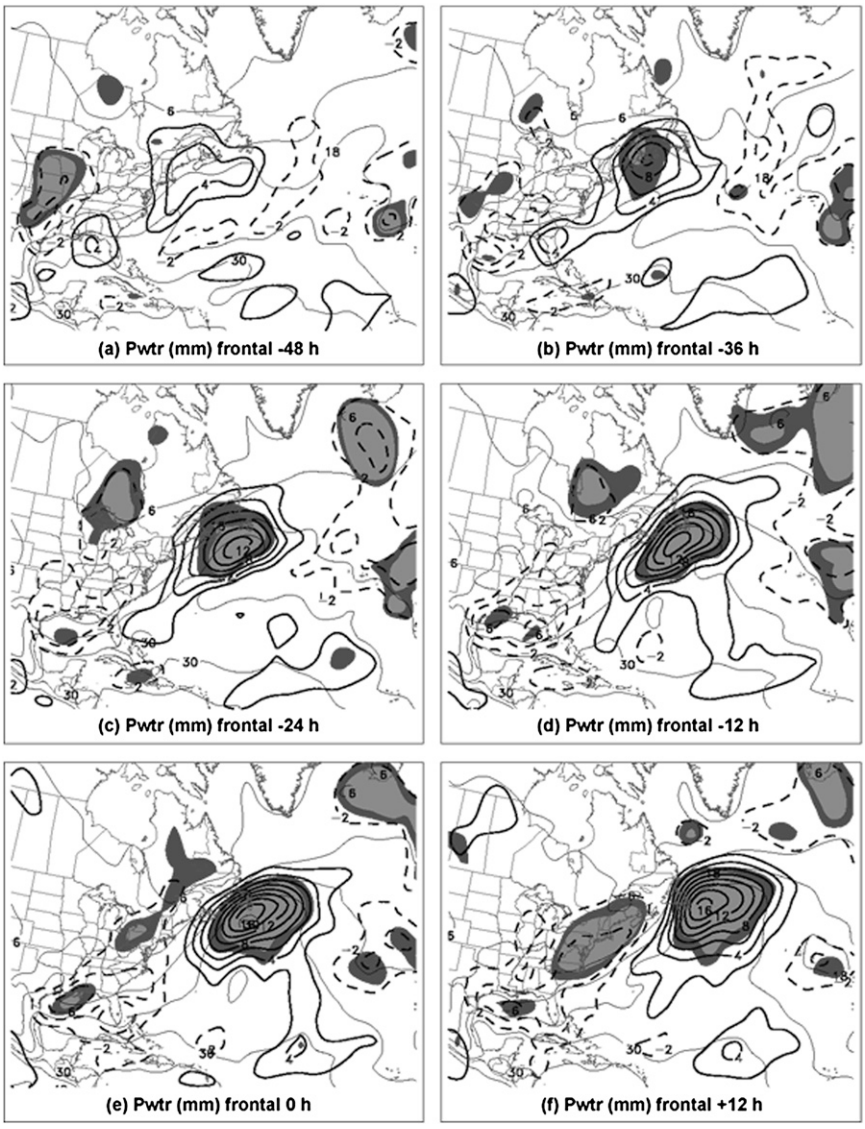

FIG. 20. As in Fig. 17, but for the frontal cases.

soundings also exhibit a relatively low tropopause, consistent with the passage of a cool-season cold-core low.

In the frontal SLP composite, a negative anomaly upstream of St. John's and positive anomaly downstream of St. John's are evident at $t = -48$ h (Fig. 18a). The origin of the negative anomaly appears to be the Great Lakes region, much farther north than the location of the surface cyclone in the cyclone composite. Moreover, while the anomalous cyclone only slightly strengthens as it moves slowly eastward toward St. John's, the downstream positive anomaly rapidly intensifies, reaching its maximum amplitude at $t = -24$ h (Fig. 18c). The intensification of the anomalous anticyclone downstream helps to set up a baroclinic zone near St. John's, facilitating secondary cyclogenesis by $t = -12$ h (Fig. 18d). This is evident in the SLP composite, as the position of the new cyclone at $t = -12$ h (Fig. 18d) is significantly to the southeast of the position of the original cyclone at $t = -24$ h (Fig. 18c). The relatively weak secondary sea level

TABLE 1. The 50 extreme cases broken down by methodology and synoptic typing.

	Cyclone ($n = 35$)	Frontal ($n = 11$)	Neither ($n = 4$)
South ($n = 11$)	4	6	1
Southwest ($n = 31$)	23	5	3
West ($n = 8$)	8	0	0

TABLE 2. Average event precipitation and synoptic characteristics associated with each trajectory type, for the 50 extreme precipitation cases.

	SLP	500-hPa height	PW
South ($n = 11$) avg. event (mm): 42.93	Strong downstream anticyclone	Intense downstream ridging	Strong southerly flow just south of St. John's
	Cyclone passes south and east of St. John's	Lack of upstream trough	Pooling of moisture
Southwest ($n = 31$) avg. event (mm): 42.17	Strong upstream cyclone passes west of St. John's	Intense upstream trough	Transient significant positive anomaly in Gulf of Mexico 2 days prior to event rapidly strengthens, moving northeastward toward St. John's
	Weak downstream anticyclone to start, slowly strengthens	Slowly building downstream ridge, possibly due to WAA and LHR	
West ($n = 8$) avg. event (mm): 42.49	Strongest cyclone of any type, passing just south and east of St. John's	No upstream trough until $t = 0$, probably associated with baroclinic instability following rapid surface development	Positive anomaly becomes statistically significant over Atlantic, just south and east of St. John's
	Alberta Clipper–like track that rapidly intensifies over Atlantic		
	Complete lack of downstream anticyclone	Lack of downstream ridge	

cyclone then proceeds to move along the east coast of North America, bringing relatively small associated values of QG forcing for ascent. This will be more explicitly detailed in future work.

The 500-hPa height composites also indicate that the upstream trough–cycloneis relatively weak. The positive height anomaly downstream of St. John's is evident as early as $t = -48$ h. This positive height anomaly proceeds to strengthen over the subsequent 48–60 h, partially in response to latent heat release from heavy precipitation at St. John's. The PW composite in the frontal group (Fig. 20) depicts a positive anomaly near Nova Scotia at $t = -36$ h (Fig. 20b). The positive PW anomaly subsequently intensifies as it moves slowly northeastward, coincidental with the stronger southerly geostrophic flow into St. John's caused by the intensification of the anticyclone downstream and the secondary cyclogenesis upstream. In sum, the frontal composite is representative of a group of events that are characterized by relatively weak midlevel vorticity advection and low-level horizontal temperature advection in a low static stability environment. The forcing for ascent provided by the low-level frontogenesis seems to be sufficient in the frontal cases provided the air mass at St. John's is characterized by particularly low static stability.

Finally, soundings at St. John's examined for the $t = -12$ h to $t = +12$ h time period depict three main differences from the cyclone composite soundings: (a) a strong boundary layer inversion and (b) a much higher tropopause, suggesting different air masses, one associated

TABLE 3. Average event precipitation and synoptic characteristics associated with each quasigeostrophic forcing type.

	SLP	500-hPa height	PW
Cyclone ($n = 35$) avg. event (mm): 42.39	Strong cyclone develops on U.S. mid-Atlantic coast and moves northeastward while strengthening rapidly	Anomalous ridge over U.S west coast 3 days prior to event	Significant positive anomaly develops off U.S. mid-Atlantic coast at $t = -36$ h, rapidly intensifies and center passes just south and east of St. John's
	Cyclone center passes directly over station	Possible downstream Rossby wave development leads to strong trough upstream of St. John's and slowly strengthening downstream ridge	
	Downstream anticyclone builds slowly		
Frontal ($n = 11$) avg. event (mm): 42.69	Strong downstream anticyclone at $t = -48$ h	Lack of upstream trough	Positive anomaly intensifies upon reaching the Atlantic at $t = -36$ h
	Weak Alberta clipper–type cyclone from Great Lakes region, redevelops to the southeast as weak frontal wave along the coast	Strong ridge downstream of St. John's at $t = -48$ h	Propagates eastward toward St. John's, with center passing just south and east

TABLE 4. The 50 cases from each precipitation amount group defined in Milrad et al. (2009), listed by trajectory classification.

	Extreme ($n = 50$)	Moderate ($n = 50$)	Light ($n = 50$)
South	11	2	4
Southwest	31	38	22
West	8	10	24

TABLE 5. The 50 cases from each precipitation amount group defined in Milrad et al. (2009), listed by QG forcing classification.

	Extreme ($n = 50$)	Moderate ($n = 50$)	Light ($n = 50$)
Cyclone	35	30	28
Frontal	11	15	10
Neither	4	5	12

with a typical cold-core low (cyclone composite) and the other a subtropical anticyclone (frontal composite).

One issue that immediately arises out of the use of two different manual typing methodologies is the extent of overlap between the two methodologies. While subcomposites have not yet been produced, the authors do hope to address this issue in future research. For now, a statistical representation of the overlap between the two methodologies is visible in Table 1. As is suggested by the identification of synoptic structures (particularly the presence of the downstream anticyclone), a significant portion of the south cases are also considered to be frontal cases. While there are minor differences between the south and frontal composites, the induced southerly geostrophic flow into St. John's is consistent in both cases. Finally, all eight of the west cases and three-quarters of the southwest cases are also part of the cyclone composite, which supports the assertion that both the southwest and west cases involve a rapidly developing upstream sea level cyclone.

The authors hope that the structures identified in this paper will be of use to the local forecaster at St. John's and similar stations. To that end, a quick reference guide to important conclusions highlighted in this paper is provided in Tables 2 and 3 for the trajectory and QG forcing types, respectively.

A final issue that arises out of the analysis in this paper is the comparison of the synoptic structures associated with a particular composite group (e.g., west trajectory events) among the different precipitation amount categories (e.g., extreme, moderate, light). Such an analysis could be quite useful to the forecaster. However, due to space concerns, the figures for the moderate and light events are not shown and the focus in this paper remains on the extreme events, since they have the greatest potential impact on St. John's. That said, Tables 4 and 5

TABLE 6. Important synoptic-scale structures and precursors associated with each trajectory composite group, among the three precipitation amount categories defined in Milrad et al. (2009).

	Extreme	Moderate	Light
South	Described in Table 2	Not enough cases	Not enough cases
Southwest	Described in Table 2	Anomalous cyclones and positive PW anomalies of similar strengths to extreme cases, but originate farther north and west Precursor 500-hPa ridge at $t = -72$ h farther north on West Coast than in extreme cases; downstream trough–ridge less amplified	Anomalous cyclone substantially weaker than in extreme and moderate cases, as well as originating farther to the north and west 500-hPa precursor ridge on West Coast substantially farther to the north than in extreme or moderate cases, while downstream trough–ridge much less amplified Lack of coherent PW anomaly until $t = -12$ h (when disturbance reaches the ocean) and weaker PW anomaly overall
West	Described in Table 2	Precursor negative SLP anomaly near St. John's at $t = -48$ h; precipitation-causing anomalous cyclone not visible until $t = -12$ h; upon reaching the ocean, farther north than in extreme cases 500-hPa trough less amplified and farther to the north than in extreme composite No precursor positive PW anomaly over central United States	Precursor negative SLP anomaly northeast of St. John's at $t = -48$ h; Alberta clipper anomalous cyclone anomaly over Minnesota at $t = -48$ h, which becomes precipitation-causing system at St. John's 500-hPa flow less amplified than extreme and moderate cases No substantial PW anomaly in central United States before event or at St. John's during event

TABLE 7. Important synoptic-scale structures and precursors associated with each QG forcing composite group, among the three precipitation amount categories defined in Milrad et al. (2009).

	Extreme	Moderate	Light
Cyclone	Described in Table 3	Negative SLP anomaly at $t = -48$ h substantially farther to the north than in extreme cases 500-hPa precursor ridge over west coast of North America at $t = -72$ h slightly farther to north, while downstream development is less amplified than in extreme cases Positive PW anomaly forms farther to the north than in extreme cases at $t = -36$ h and is more intense upon reaching St. John's ($t = 0$ h)	Cyclone intensifies upon reaching Atlantic at $t = 0$ h 500-hPa precursor ridge at $t = -72$ h over Pacific northwest similar to moderate cases; East Coast trough weaker and farther north than in moderate and extreme cases Weaker PW anomaly not seen until $t = -12$ h, later than moderate cases
Frontal	Described in Table 3	Much weaker downstream sea level anticyclone than in extreme cases → weaker southerly geostrophic flow Downstream 500-hPa ridge weaker and farther south than in extreme cases → flow much less amplified Positive PW anomaly, farther south of St. John's than in extreme cases, likely due to slightly different position of anticyclone	Anomalous sea level anticyclone–midlevel ridge east of St. John's farther north than moderate cases; similar structures to extreme cases but appears later and is slightly weaker Upstream anomalous cyclone weaker than moderate cases; positive PW anomaly much weaker than in extreme and moderate composites

display statistics for the different precipitation amount categories defined in Milrad et al. (2009), broken down by composite group. In addition, Tables 6 and 7 serve as a summary of important structural differences for each composite group in this paper, among the different precipitation threshold categories. The findings include the following points (which are fully described in Tables 6 and 7):

- The track of the cyclone in the southwest cases and position of the precursor ($t = -72$ h) west coast ridge are farther to the north and west in the moderate and light cases than in the extreme composite.
- The precursor positive PW anomaly seen over the midwestern United States in the extreme west trajectory composites is not present in either the moderate or light west trajectory cases.
- In the cyclone group, both upper-level and sea level synoptic structures are located farther to the north and west in the moderate and light cases than in the extreme composite.
- The downstream ridging and corresponding surface high that are seen in the extreme frontal cases are much stronger than in the moderate and light frontal cases.

Synoptic composite plots for the various synoptic types (both partitioning methodologies) are available online (http://www.meteo.mcgill.ca/~milrad/Milrad2009b.htm).

In the future, detailed case studies of recent extreme precipitation events at St. John's will be produced, synoptically typing the events into the categories defined in this paper, while also explicitly detailing the associated dynamics.

Acknowledgments. This research has been supported by grants from the Natural Sciences and Engineering Research Council of Canada and the Canadian Foundation for Climate and Atmospheric Sciences. Many thanks are due to the three anonymous reviewers for their input and suggestions. Also, special thanks to the National Centers for Environmental Prediction (NCEP) and the National Climatic Data Center (NCDC) for providing access to the NCEP Global Reanalysis. Finally, thanks to Gerard Morin at the Atlantic Climate Centre of Environment Canada for providing the 6-hourly precipitation data.

REFERENCES

Bao, J. W., S. A. Michelson, P. J. Neiman, F. M. Ralph, and J. M. Wilczak, 2006: Interpretation of enhanced integrated water vapor bands associated with extratropical cyclones: Their formation and connection to tropical moisture. *Mon. Wea. Rev.,* **134,** 1063–1068.

Bluestein, H., 1992a: *Principles of Kinematics and Dynamics.* Vol. 1, *Synoptic Dynamic Meteorology in Midlatitudes,* Oxford University Press, 431 pp.

——, 1992b: *Observations and Theory of Weather Systems*. Vol. 2, *Synoptic–Dynamic Meteorology in Midlatitudes,* Oxford University Press, 594 pp.

Frakes, B., and B. Yarnal, 1997: A procedure for blending manual and correlation-based synoptic classifications. *Int. J. Climatol.,* **17,** 1381–1396.

Grumm, R. H., and R. Hart, 2001: Standardized anomalies applied to significant cold season weather events: Preliminary findings. *Wea. Forecasting,* **16,** 736–754.

Gyakum, J. R., and E. S. Barker, 1988: A case study of explosive subsynoptic-scale cyclogenesis. *Mon. Wea. Rev.,* **116,** 2225–2253.

Hoskins, B. J., I. Draghici, and H. C. Davies, 1978: A new look at the ω equation. *Quart. J. Roy. Meteor. Soc.,* **104,** 31–38.

Jones, P. D., M. Hulme, and K. R. Briffa, 1993: A comparison of Lamb circulation types with an objective classification scheme. *Int. J. Climatol.,* **13,** 655–663.

Kalnay, E., and Coauthors, 1996: The NCEP/NCAR 40-Year Reanalysis Project. *Bull. Amer. Meteor. Soc.,* **77,** 437–471.

Keyser, D., M. J. Reeder, and R. J. Reed, 1988: A generalization of Petterssen's frontogenesis function and its relation to the forcing of vertical motion. *Mon. Wea. Rev.,* **116,** 762–780.

Knippertz, P., and J. E. Martin, 2007: A Pacific moisture conveyor belt and its relationship to a significant precipitation event in the semiarid southwestern United States. *Wea. Forecasting,* **22,** 125–142.

Koch, S., M. DesJardins, and P. Kocin, 1983: An interactive Barnes objective map analysis scheme for use with satellite and conventional data. *J. Appl. Meteor.,* **22,** 1487–1503.

Ladd, J. W., and D. M. Driscoll, 1980: A comparison of objective and subjective means of weather typing: An example from west Texas. *J. Appl. Meteor.,* **19,** 691–704.

Martin, J. E., 2006: *Mid-Latitude Atmospheric Dynamics*. John Wiley and Sons, 324 pp.

Mekis, E., and W. D. Hogg, 1999: Rehabilitation and analysis of Canadian daily precipitation time series. *Atmos.–Ocean,* **37,** 53–85.

Mesinger, F., and Coauthors, 2006: North American Regional Reanalysis. *Bull. Amer. Meteor. Soc.,* **87,** 343–360.

Milrad, S. M., E. A. Atallah, and J. R. Gyakum, 2009: Synoptic-scale characteristics and precursors of cool-season precipitation events at St. John's, Newfoundland, 1979–2005. *Wea. Forecasting,* **24,** 667–689.

Muller, R. A., 1977: A synoptic climatology for environmental baseline analysis: New Orleans. *J. Appl. Meteor.,* **16,** 20–33.

——, and A. L. Jackson, 1985: Estimates of climatic air quality potential at Shreveport, Louisiana. *J. Climate Appl. Meteor.,* **24,** 293–301.

Overland, J. E., and T. R. Hiester, 1980: Development of a synoptic climatology for the northeast Gulf of Alaska. *J. Appl. Meteor.,* **19,** 1–14.

Reap, R. M., 1972: An operational three-dimensional trajectory model. *J. Appl. Meteor.,* **11,** 1193–1202.

Roberge, A., J. Gyakum, and E. Atallah, 2009: Analysis of intense poleward water vapor transports into high latitudes of western North America. *Wea. Forecasting,* **24,** 1732–1747.

Roebber, P. J., and L. F. Bosart, 1998: The sensitivity of precipitation to circulation details. Part I: An analysis of regional analogs. *Mon. Wea. Rev.,* **126,** 437–455.

Sheridan, S. C., 2002: The redevelopment of a weather-type classification scheme for North America. *Int. J. Climatol.,* **22,** 51–68.

Sisson, P. A., and J. R. Gyakum, 2004: Synoptic-scale precursors to significant cold-season precipitation events in Burlington, Vermont. *Wea. Forecasting,* **19,** 841–854.

Stewart, R. E., R. W. Shaw, and G. A. Isaac, 1987: Canadian Atlantic Storms Program: The meteorological field project. *Bull. Amer. Meteor. Soc.,* **68,** 338–345.

Uccellini, L. W., D. Keyser, K. F. Brill, and C. H. Wash, 1985: The Presidents' Day cyclone of 18–19 February 1979: Influence of upstream trough amplification and associated tropopause folding on rapid cyclogenesis. *Mon. Wea. Rev.,* **113,** 962–988.

Wernli, H., 1997: A Lagrangian-based analysis of extratropical cyclones. II: A detailed case study. *Quart. J. Roy. Meteor. Soc.,* **123,** 467–489.

——, and H. C. Davies, 1997: A Lagrangian-based analysis of extratropical cyclones. I: The method and some applications. *Quart. J. Roy. Meteor. Soc.,* **123,** 467–489.